 doi:10.20944/preprints202104.0048.v1

Type of the Paper: Article

In-situ flexibility of both redox-states of the chloroplast regulatory protein CP12

Helene Launay*[1], Hui Shao[1], Olivier Bornet[2], Francois-Xavier Cantrelle[3,4], Regine Lebrun[5], Veronique Receveur-Brechot[1] and Brigitte Gontero*[1]

[1] Aix Marseille Univ., CNRS BIP UMR 7281, 31 chemin Joseph Aiguier, 13402, Marseille Cedex 20, France; HL : helene.launay@univ-amu.fr, HS : lanqiqiaopan@163.com; VRB : vbrechot@imm.cnrs.fr; BG : bmeunier@imm.cnrs.fr

[2] NMR Platform, Institut de Microbiologie de la Méditerranée, CNRS, Aix Marseille Univ., 13009 Marseille, France; bornet@imm.cnrs.fr

[3] CNRS, ERL9002, Integrative Structural Biology, Lille, France

[4] University of Lille, INSERM, CHU Lille University Hospital, Institut Pasteur de Lille, UMR1167, Lille, France, francois-xavier.cantrelle@univ-lille.fr

[5] Plate-forme Protéomique, Marseille Protéomique (MaP), IMM FR 3479, 31 Chemin Joseph Aiguier 13009 Marseille, France, rlebrun@imm.cnrs.fr

* Correspondence: HL: helene.launay@univ-amu.fr ; BG: bmeunier@imm.cnrs.fr

Abstract: In the chloroplast, Calvin-Benson-Bassham enzymes are active in the reducing environment imposed in the light via the electrons from the photosystems. In the dark these enzymes are inhibited, and this regulation is mainly mediated via oxidation of key regulatory cysteine residues. CP12 is a small protein that plays a role in this regulation with four cysteine residues that undergo a redox transition. Using amide-proton exchange with solvent measured by nuclear magnetic resonance (NMR) and mass-spectrometry, we confirmed that reduced CP12 is intrinsically disordered. Using real-time NMR, we showed that the oxidation of the two disulfide bridges are simultaneous. In oxidized CP12, the C_{23}-C_{31} pair is in a region that undergoes a conformational exchange in the NMR-intermediate timescale. The C_{66}-C_{75} pair is in the C-terminus that folds into a stable helical turn. We confirmed that these structural states exist in a physiologically relevant environment that is, in cell extract from *Chlamydomonas reinhardtii*. Consistent with these structural equilibria, the reduction is slower for the C_{66}-C_{75} pair compared to the C_{23}-C_{31} pair. Finally, the redox mid-potentials for the two cysteine pairs differ and are similar to those found for phosphoribulokinase and glyceraldehyde 3-phosphate dehydrogenase, that we relate to the regulatory role of CP12.

Keywords: Calvin-Benson-Bassham cycle; Conditionally disordered protein; Intrinsically disordered protein; photosynthesis regulation.

1. Introduction

Redox regulation based on disulfide-dithiol exchanges constitutes a rapid and reversible post translational modification (PTM) that affects protein conformation. PTM in intrinsically disordered regions (IDRs) can confer flexibility or in contrast order, thereby allowing quick response to a stimulus for a rapid regulation process in cell. The proteins with disorder triggered by different stimuli (redox, pH, temperature…) are categorized as conditionally disordered proteins (CDPs) [1]. PTMs on CDPs can contribute to the diversification and functionality of proteomes, by regulating different properties of proteins and this is termed "proteoform concept" [2]. Among these CDPs, some are particularly sensitive to redox changes, and these have been termed redox-dependent CDPs [3]. In these CDPs, key cysteine residues can be either involved in disulfide bridge or not, depending on the redox conditions. Among the twenty natural amino acid residues, cysteine was believed to be the more order promoting residue, however many examples proteins containing IDRs, or intrinsically disordered proteins (IDP) have been described in the literature that contain redox-sensitive cysteine

Preprints (www.preprints.org) | NOT PEER-REVIEWED | Posted: 2 April 2021 doi:10.20944/preprints202104.0048.v1

residues pair. To cite but a few examples, Hsp33 undergoes an order-to-disorder transition upon oxidation [4,5], and Cox17 and its partner Mia40 undergo a disorder-to-order transition upon oxidation [6,7].

The chloroplasts of photosynthetic organisms are submitted to an important decrease of their redox potential (more reducing conditions) upon dark to light transition and reciprocally an increase of the redox potential (more oxidizing conditions) upon light to dark transitions. Many enzymes are regulated by different PTM such as S-glutathionylation or S-nitrosylation but mainly through redox modulators via thiol-disulfide interconversions involving the ubiquitous thioredoxins (Trx) [8–10]. Light has a dual role and activates enzymes involved in carbohydrate synthesis while inhibiting enzymes involved in their degradation, avoiding futile cycling. For instance, to enzymes that are playing major role in the carbohydrate breakdown are inhibited in the light: the glucose-6-phosphate dehydrogenase involved in the oxidative pentose phosphate pathway [11,12] and the phosphofructokinase (PFK) involved in the glycolysis [13,14]. For example, in *Arabidopsis thaliana*, the isoform PFK5 was shown to be reduced by Trx f and oxidized and activated by a recently identified NADPH dependent Trx-like2/2-Cys peroxiredoxin pathway which is branched to the ferredoxin NADP reductase [14,15]. In contrast, the Calvin-Benson-Bassham (CBB) cycle that is responsible for CO_2 assimilation and carbohydrate synthesis, is inactive under dark and only operates in the light. Activation as well as inhibition of CBB enzymes have been shown to be very quick within 30s [16–19]. The mechanism of activation has been intensively studied and is mainly under the control of Trxs through the ferredoxin-Trx system [20]. The inhibition mechanism also involves the ferredoxin-Trx system as well as the newly described Trx-like2/2-Cys peroxiredoxin pathway [15,20].

Redox regulation of enzymes of the CBB cycle can be either direct via their regulatory cysteine residues (e.g. phosphoribulokinase (PRK), sedoheptulose-1,7-bisphosphatase, fructose1,6-bisphosphatase, [21]) or indirect via redox mediators such as the chloroplast protein CP12. This protein of about 8.5 kDa is able to act as a switch on/off of this pathway, upon light to dark transition and reciprocally [22,23]. This protein has four cysteine residues that form two disulfide bridges under dark allowing the formation of a supramolecular complex between two enzymes of the CBB cycle. The N-terminal disulfide bridge C_{23}-C_{31} is proximal with the region that is essential for PRK-association W_{35}xxVEExxxxxxH_{47} [24], and the C-terminal disulfide bridge C_{66}-C_{75} is within the region that interacts with glyceraldehyde-3-phosphate dehydrogenase (GAPDH) [25,26]. When embedded in this ternary complex, the two enzymes are inactive and the CBB cycle is not functioning. In contrast, upon dark to light transition, the two disulfide bridges of CP12 become reduced and the ternary complex dissociates releasing active enzymes and the CBB cycle can operate. CP12 is present in most photosynthetic organisms [27,28] and has features of disordered proteins. In the green alga, *Chlamydomonas reinhardtii* as well as in other organisms, this protein is fully disordered under its reduced state ($CP12_{red}$) and bears some secondary structural elements under oxidized state though being flexible (Figure 1) [29–31]. The C-terminal region that surrounds the C_{66}-C_{75} disulfide bridge folds into a stable α-helical turn. It is preceded by a disordered linker and a highly dynamical N-terminal region that contains the C_{23}-C_{31} cysteine pair. CP12 belongs to the CDP family and its conditional disorder allows for nuanced control of CBB enzymes and their fine regulation through binding processes. Besides the dark down regulation of CBB enzymes, this protein is a jack-of–all trades and can perform different functions in photosynthetic cell [22,32].

Some structural data *in-vitro* have been obtained in the last few years (Figure 1) [25,26,29,31] but, as for many IDP and CDP, the flexibility of the protein in its physiological milieu remains to be confirmed [33,34]. Indeed, in-cell, the molecular crowding and the presence of interacting partners can have a significant contribution to the conformational sampling of an IDP, as it has been shown on well-studied IDPs such as tau and alpha-synuclein [35,36]. That is also the case for CDP, and redox dependent disorder-to-order transition of Mia40 and Cox17 has been shown in isolation and within HeLa cell cytoplasm [37,38]. Nevertheless, the effect of the complex physiological environment has never been studied on the model CDP, CP12.

Preprints (www.preprints.org) | NOT PEER-REVIEWED | Posted: 2 April 2021 doi:10.20944/preprints202104.0048.v1

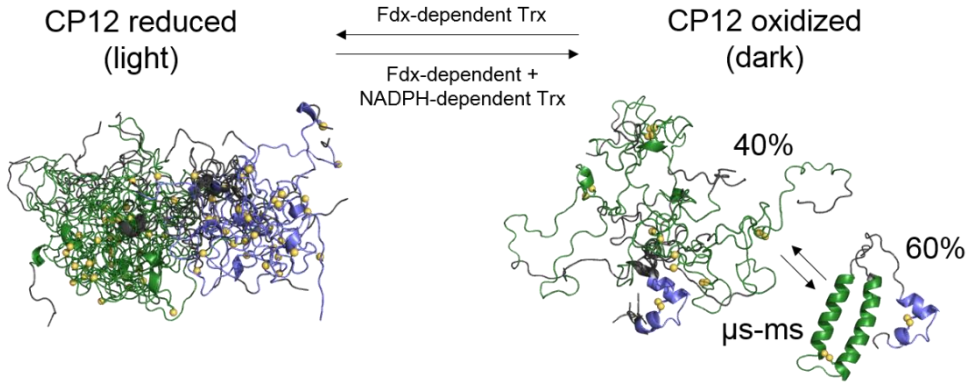

Figure 1: Model of the redox-transition of CP12. The structural models are derived from Launay et al [30,31]. The complex Trx network is derived from Cejudo et al [15]. The sulphur atoms of the two pairs of cysteine residues are in yellow. Trx and Fdx stand for thioredoxins and ferredoxin respectively.

The objective of this study was to monitor the structural and redox properties of both cysteine residues pairs depending on the physical-chemical conditions. In order to understand better the redox-dependent conformational sampling of CP12 *in vitro*, the amide proton exchange rates were measured by mass-spectrometry and Nuclear Magnetic Resonance (NMR), as well as the temperature and pH variation of the NMR observables. The conformational states of both cysteine residues pair regions in $CP12_{ox}$ and $CP12_{red}$ were also observed into more physiological conditions, in *C. reinhardtii* cell extracts. We thus confirmed the distinct dynamical nature of both cysteine residues pair regions *in-situ* with all the possible interacting partners, PTM mediators, or solubilizing molecules present in the cell extract. Since, as mentioned above, it is the CP12 redox transition that governs the GAPDH and PRK regulation, we monitored in-real time the redox transition of CP12 in isolation and within *C. reinhardtii* cell extract, and determined the oxidation-reduction midpoint potentials of its two pairs of cysteine residues.

2. Materials and Methods

2.1. Amide-water proton exchange kinetic measurements by NMR

The kinetics of amide-water proton exchange was measured on $CP12_{red}$ (in the presence of 20 mM DTT_{red}) and $CP12_{ox}$ in 50mM NaPi pH 6.5, 50mM NaCl, 1mM EDTA, 5% D_2O, with traces of sodium trimethylsilylpropanesulfonate (DSS) by NMR using the CLEANEX-PM [39] pulse sequence on a 600MHz Advance III spectrometer equipped with a cryoprobe, pH 7.0 and pH 6.0 and at 283K, with the following spin-lock delays (τ_m in ms): 1.6, 3.2, 6.5, 9.7, 20, 39 and 81 and as a pseudo-3D experiments. The signal integral for each residue ($V_{\tau m}$) was normalized against that in a fast-HSQC spectrum (V_0) acquired using the same parameters, that is a ^{15}N acquisition time of 42ms, a ^{1}H acquisition time of 243 ms, and 64 scans. The spectra were transformed in nmrPipe [40], and the cross-peak integrals measured using NMRFAM-SPARKY[41]. The increase of resonance integral as a function of the spin-lock delay (τ_m) was fitted to the following equation using a Levenberg-Marquardt nonlinear regression function in Octave[42]:

$$\frac{V_{\tau m}}{V_0} = \frac{k}{R_{1A,app} + k - R_{1B,app}} \times \left\{\exp\left(-R_{1B,app} \times \tau_m\right) - \exp\left[-\left(R_{1A,app} + k\right).\tau_m\right]\right\} \quad (1)$$

where $R_{1B,app}$ is the apparent water relaxation rate and is set to $0.6s^{-1}$, and k (the water-amide exchange rate) and $R_{1A,app}$ (the amide relaxation rate) are optimized. The fits are shown in Sup. Fig. 1. The exchange rate (k_{ex}) is set to k/0.85 to take into account the water saturation effect in the CLEANEX-PM experiment [39,43]. The uncertainties on k_{ex} values are obtained by repeating the

Preprints (www.preprints.org) | NOT PEER-REVIEWED | Posted: 2 April 2021 doi:10.20944/preprints202104.0048.v1

optimization upon randomly varying the experimental integrals within 10% error (which is an overestimation of the experimental error). The intrinsic rates of exchange (k_{int}) were predicted using Sphere (https://protocol.fccc.edu/research/labs/roder/sphere/) [44].

2.2. Gibbs-free energy derived from protection factors

The protection factor for $CP12_{ox}$ (P) is calculated with:

$$P = \frac{k_{ex,oxidized\ state}}{k_{ex,reduced\ state}} \quad (2)$$

The Delta Gibbs free energy for the backbone structure of oxidized CP12 is calculated from P with the following equation:

$$\Delta G = -RT \ln(P) \quad (3)$$

with R the gas constant ($1.987\ 10^{-3}$ $kcal.K^{-1}.mol^{-1}$) and T the temperature (293 K).

2.3. Amide-water proton exchange kinetic measurements by mass-spectrometry

Mass-spectrometry was also used to monitor the rate of exchange of proton amide with deuterated solvent. $CP12_{ox}$ and $CP12_{red}$ in 15 mM Tris pH 6.6, 50 mM NaCl were diluted 10x in either 10 mM potassium phosphate in 100% H_2O, pH 7.0 for control "undeuterated" experiments, or 10 mM potassium phosphate in 99.96% D_2O, pD 7.0 for the "deuterated" experiments. pH values of D_2O solutions were adjusted to the corresponding pD values using the equation (pD = pHread + 0.40). Final concentration of $CP12_{ox}$ and $CP12_{red}$ was 17 µM and 20 µM, respectively. The samples were left from 10 s to 15 min for the exchange to occur. At different times, the exchange reaction was quenched by diluting twice in pre-chilled 100 mM potassium phosphate, pH 2.66 containing 2 mM Tris(2-carboxyethyl)phosphine (TCEP), and immediately injected on a nanoACQUITY UPLC™ system with HDX technology (Waters Corporation, Milford, MA, USA). The proteins were online digested at 20°C in an immobilized pepsin column (2.1 × 30 mm, Applied Biosystems, CA, USA) for 5 min in 0.1% formic acid/ H_2O at a flow rate of 100 µL/min. Peptides were subsequently trapped and desalted online using an ACQUITY UPLC® BEH C18 VanGuard™ Pre-column (1.7 µm, Waters) at 0◦C, then eluted into an ACQUITY UPLC® BEH C18 column (1.7 µm, 1 mm × 100 mm, Waters) held at 0 ◦C, and separated with a linear acetonitrile gradient containing 0.1% formic acid. Mass spectra were acquired on a SYNAPT-G1 mass spectrometer (Waters) with an electrospray ionization source and lock-mass corrected by a Glu-fibrinogen peptide solution, in MSe mode, over the m/z range of 50–2,000. Undeuterated peptides were identified using ProteinLynx Global Server software 3.1 (Waters). Deuterium uptake data for each peptic peptide from the "deuterated" experiments were automatically calculated using DynamX 2.0 software (Waters) and the results were manually checked.

2.4. Temperature dependence of the NMR chemical shift and signal intensity

^{1}H-^{15}N fast-HSQC of $CP12_{ox}$ (400 µM) in 50mM NaPi pH 6.5, 50mM NaCl and with 20 mM DTT_{ox}, 5% D_2O were recorded at varying temperature (277K, 284K, 291K, 298K, 305K, 313K, 319K), with a proton acquisition time of 243.3 ms and a ^{15}N acquisition time of 42 ms on a 600MHz and a 900MHz Advance III spectrometer equipped with cryo-probes. When mentioned, one equivalent of copper ($CuSO_4$) was added to the sample to catalyze oxidation, followed by the addition of 1 mM EDTA and dialysis. The samples recorded at varying pH were recorded in 20 mM Tris, and pH was increased by the addition of NaOH. The spectra were processed with nmrPipe [40] with Sine Bell window function. The referencing of the spectra were done using the frequency of water (carrier frequency) at these temperature [40], and controlled via the chemical shift of DSS, with uncertainty bellow 0.05ppm. The chemical shift of all CP12 amide protons, as well as the signal intensity were determined in NMRFAM-SPARKY [41], and exported in Octave [42]. The chemical shift dependence with temperature was fitted with the following equation:

$$\delta\ ^{1}H\ (T) = slope \times T + c \quad (4)$$

Preprints (www.preprints.org) | NOT PEER-REVIEWED | Posted: 2 April 2021 doi:10.20944/preprints202104.0048.v1

where c is a constant, T the temperature in K.

2.5. Thermodynamic of the redox transition

The redox mid-potentials for the transition for each pair of cysteine residues were probed by NMR as proposed in [45]. 50 µM of CP12 in 50mM NaPi pH 6.5, 50mM NaCl, pH 7 were prepared with addition of 20 mM DTT with a varying ratio of DTT_{ox} and DTT_{red} in a glovebox under anaerobic atmosphere. The samples were left overnight at ambient temperature to reach the equilibrium. The ratios of DTT_{ox} and DTT_{red} were controlled by NMR using the proton signal intensity at 2.85 and 3.05 ppm (DTT_{ox}) and at 2.6 ppm (DTT_{red}). ^{1}H-^{15}N fast-HSQC of each sample were recorded. The electropotential for each sample was calculated from the ratio of the concentrations of DTT_{ox} over DTT_{red} using the Nernst equation [45]:

$$E_{h,\ pH\,7} = E^{0}_{DTT,\ pH\,7} + \frac{RT}{nF} \times \ln\left(\frac{[DTT_{ox}]}{[DTT_{red}]^{2}}\right) \quad (5)$$

where $E_{DTT,\ pH7}$ is the redox mid-potential of DTT (-332 mV [45,46]), R is the gas constant (1.987 10^{-3} $kcal.K^{-1}.mol^{-1}$) and T is the temperature (283 K), n is the number of electrons (2), and F is the Faraday constant (95484.6 $J.V^{-1}.mol^{-1}$).

^{1}H-^{15}N fast HSQC were recorded at 283K for all samples, the data were transformed in nmrPipe [40], and the signal intensity at frequency of reduced C_{23} ($\delta^{15}N$: 117.632 ppm, $\delta^{1}H$: 8.282 ppm), reduced C_{31} ($\delta^{15}N$: 119.451 ppm, $\delta^{1}H$: 8.205 ppm), reduced C_{66} ($\delta^{15}N$: 121.895 ppm, $\delta^{1}H$: 8.284 ppm), reduced C_{75} ($\delta^{15}N$: 120.418 ppm, $\delta^{1}H$: 8.471 ppm), oxidized C_{66} ($\delta^{15}N$: 115.784 ppm, $\delta^{1}H$: 8.696 ppm) and oxidized C_{75} ($\delta^{15}N$: 116.351 ppm, $\delta^{1}H$: 7.948 ppm) were obtained in NMRFAM-Sparky [41]. The signal intensity of the reduced resonance as a function of the electropotential was fitted in Octave using the following sigmoidal function [46]:

$$\frac{I}{I_0} = \frac{1}{1 + exp\left[0.2 \times \left(E_{h,\ pH7} - E^{0}_{Cysteine}\right)\right]} \quad (6)$$

The signal intensity of the oxidized resonance as a function of the electropotential was fitted using the following sigmoidal function [46]:

$$\frac{I}{I_0} = 1 - \frac{1}{1+exp\left[0.2\times\left(E_{h,\ pH7} - E^{0}_{Cysteine}\right)\right]} \quad (7)$$

The same experiment was repeated at pH 8 in 30mM Tris, 50mM NaCl. The redox potential of DTT is expected to change as a function of pH using the following equation [45]:

$$E^{0}_{DTT,\ pH\,8} = E^{0}_{DTT,\ pH\,7} - 59.1\ mV \quad (8)$$

and was modified consequently in equations 5, 6 and 7.

2.6. Real-time monitoring of the reduced-to-oxidized transition

20 mM DTT_{red} was added to 1 mM CP12 (50mM NaPi pH 6.5, 50mM NaCl, pH 7, 5% D_2O), the sample was left overnight to ensure complete reduction of its cysteine residues. The absence of oxidized cysteine was monitored by the acquisition of a ^{1}H-^{15}N HSQC. The reducing agent was then removed by a PD10 column, followed by dialysis (using 10 kDa cut-off vivaspin concentrators) with a buffer to which air was bubbled for one hour to oxidize the buffer. A series of ^{1}H-^{15}N fast-HSQC was then recorded at 293 K. All spectra were transformed in nmrPipe [40], and the signal intensity at frequency of reduced C_{23}, C_{31}, C_{66}, C_{75} and oxidized C_{66} and C_{75} were obtained using the autoFit.tcl script in nmrPipe [40]. The oxidized C_{23} and C_{31} resonances are broadened beyond detection [31]. The intensities were then transferred into Octave [42], and the decrease in intensity of the reduced resonances as a function of time were fitted with the following equation using Levenberg-Marquardt nonlinear regression function:

$$I/I_0 = e^{-k_{red\rightarrow ox}t} + c \quad (9)$$

Preprints (www.preprints.org) | NOT PEER-REVIEWED | Posted: 2 April 2021 doi:10.20944/preprints202104.0048.v1

where c is a constant, k the rate constant of the oxidation of the cysteine residues pair.

The increases in intensity of the oxidized resonance as a function of time were fitted with the following equation:

$$I/I_0 = c - e^{-k_{red\rightarrow ox}t} \quad (10)$$

where c is a constant, k the rate constant of the oxidation of the cysteine residues pair.

2.7. Real-time monitoring of the reduction

20 mM DTT_{red} was added a 400 µM $CP12_{ox}$ (50mM NaPi pH 6.5, 50mM NaCl, 1mM EDTA, 5% D_2O). A series of ^1H-^{15}N fast-HSQC was then recorded at 293 K. The spectra were analyzed, and the data were fitted as above. The decrease of oxidized resonance intensity as a function of time was fitted with the following equation:

$$I/I_0 = e^{-k_{ox\rightarrow red}t} + c \quad (11)$$

where c is a constant, k is the rate constant of reductions of disulfide bridges.

The increases in intensity of the reduced resonance as a function of time were fitted with the following equation:

$$I/I_0 = c - e^{-k_{ox\rightarrow red}t} \quad (12)$$

where c is a constant, k is the rate constant of reductions of disulfide bridges.

2.8. Cell extract preparation

C. reinhardtii CC124 cells were cultured at ambient temperature (22 °C), with a light/dark cycle, 110 rpm rotation for five days until they reached an absorbance at 680 nm of 1.24 (18.10^6 cells.mL^{-1}). 50 mL of culture were centrifuged at 2000 g for 15 min at 4°C and resuspended in 1 mL of buffer 30mM Tris pH 7.0, 20mM DTT_{red}, protease inhibitor Complete EDTA free (Roche) following the recommended concentration. The sample was again centrifuged 2000 g for 15 min at 4°C, and resuspended in 300 µL of the same buffer and D_2O was added to the sample. The sample was sonicated twice one min on ice. 15 µL of $CP12_{red}$ was added to reach a final concentration of 50 µM. The total protein concentration in the sample was measured using Bradford assay [47]. ^1H-^{15}N fast-HSQC of the sample was recorded at 283 K, with proton acquisition time of 243 ms, and nitrogen acquisition time of 42 ms, on a 600 MHz Advance III NMR spectrometer equipped with a cryo-probe. The data were transformed in nmrPipe [40] and signal intensity for each resonance was acquired in NMRFAM-Sparky [41].

For the oxidized sample, the same procedure was applied with the following modification: *C. reinhardtii* cells were left 24 hrs in the dark before collection. 20 mM DTT_{ox} was added to the sample instead of DTT_{red}, as well as 0.1 mM 3-(3,4-dichlorophenyl)-1,1-dimethylurea (DCMU) (Durion). 15 µL of $CP12_{ox}$ was added to reach a final concentration of 50 µM.

2.9. Diffusion coefficient determination

In the presence of cell extract, the translational diffusion coefficients of CP12 were recorded using DOSY-NMR selectively on the ^{15}N labelled protein using the heteronuclear stimulated echo experiment (XSTE) from Ferrage et al [48]. Ten experiments were recorded in a pseudo-2D fashion using bipolar square gradients of 1.4 ms (δ) of strength varying from 2 to 98% of the maximum gradient strength (G, $G_{100\%}$ = 0.5146 $T.m^{-1}$) with a fixed diffusion delay of 200 ms (Δ).

In the absence of cellular extract, the same experiment was used to probe for the translational diffusion delay of isolated CP12, and the result was compared with that obtained using standard bipolar stimulated echo experiment (STE) diffusion experiment using the same parameter. The translational diffusion coefficients were identical within 4% uncertainty.

The date were processed in nmrPipe [40] and fitted to the Stejskal-Tanner equation in Octave [42]:

Preprints (www.preprints.org) | NOT PEER-REVIEWED | Posted: 2 April 2021 doi:10.20944/preprints202104.0048.v1

$$\frac{I}{I_0} = exp\left[D \times \left(\Delta - \frac{\delta}{3}\right) \times (\delta . G . \gamma_H)\right] \quad (13)$$

where δ, Δ and G are the gradient duration, diffusion delay and gradient strengths defined above. γ_H is the proton gyromagnetic ratio (2.67 10^8 rad.s^{-1}.T^{-1}). The hydrodynamic radius associated with the diffusion coefficient was determined using the Stokes-Einstein equation:

$$r_h = \frac{k_B . T}{6\pi . D . \eta_{(T)}} \quad (14)$$

where k_B is the Boltzmann constant, T the temperature in Kelvin and η the viscosity.

2.10. Determination of delta-Gibbs free energy of binding

The delta-Gibbs free energy for binding of $CP12_{ox}$ to its partner is determined from the following equation:

$$\Delta G = \mathrm{RT} \times \ln\left(\frac{[CP12][partner]}{[complex]}\right) = \mathrm{RT} \times \ln(K_D) \quad (15)$$

where R is the gas constant (1.987 10^{-3} kcal.K^{-1}.mol^{-1}) and T is the temperature (283 K). The dissociation constant for the CP12-PRK complex is 1.3 µM, for the CP12-GAPDH complex is 0.4 nM and for the PRK-(CP12-GAPDH) complex is 60 nM [23].

3. Results

3.1. Structural transition of the region encompassing the C_{66}-C_{75} disulfide bridge upon oxidation of the isolated protein.

We first investigated the dynamics of $CP12_{red}$ by measuring the amide proton exchange rate with H_2O by NMR on $CP12_{red}$ to probe for the protected and exposed backbone amide protons. The measured k_{ex} rates were related to very fast amide-water exchange (on the order of 6.10^{-2} to 3 s^{-1}) and were only slightly slower than the predicted ones using SPHERE (Figure 2a, Figure S1 and S2), in a quasi-uniform manner. These data confirm that in its reduced state, CP12 is highly disordered [30] with amide proton exposed to the solvent, and the rate-limiting step of the exchange is the intrinsic proton exchange rate [49].

Upon oxidation, only a small subset of protons was protected as compared to the reduced state; they are all in the region that surrounds the C_{66}-C_{75} disulfide bridge. Residues E_{63} to D_{68} and E_{74} to Y_{78} for which the exchange rates were beyond our detection limit, and A_{69} and A_{72} for which exchange rates showed proton exchange rates significantly lower than in the fully disordered $CP12_{red}$. Assuming that the rate limiting step for this exchange is the unfolding of the stable helical turn, these exchange rates can be related to protection factors (Figure 2b). These protection factors are in good agreement with our previously described C-terminal structure [31], with the most protected amide being within the two small helical structures connected by the disulfide bridge (Figure 2c).

Interestingly, the variation of proton chemical shift according to the temperature for the same set of $CP12_{ox}$ residues (E_{63}, F_{65}, K_{67}, D_{68}, A_{69}, A_{72}, C_{75} and R_{76}) had slope more positive than -4.6.10^{-3} ppm.K^{-1} (Figure 2d, Figure S4), which is also indicative of hydrogen bond [50]. Together, these data confirm that the C-terminal region surrounding the C_{66}-C_{75} disulfide bridge folds in a helical turn stabilized by H-bonds upon oxidation [31].

Preprints (www.preprints.org) | NOT PEER-REVIEWED | Posted: 2 April 2021 doi:10.20944/preprints202104.0048.v1

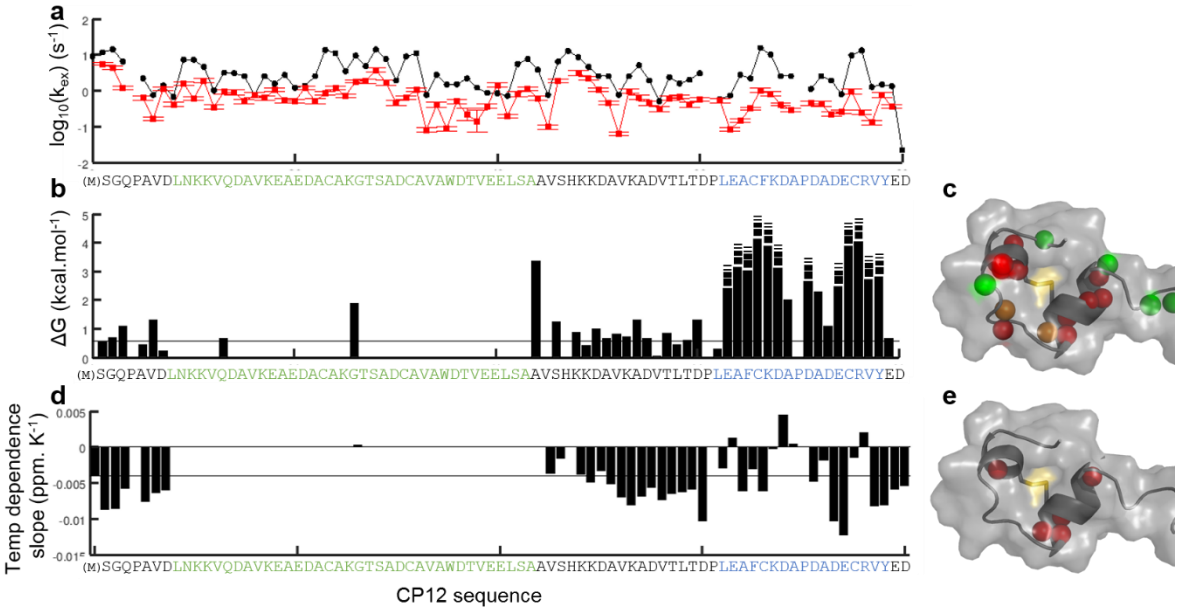

Figure 2: Labile amide protons in CP12red and CP12ox. (**a**) Solvent-amine intrinsic proton exchange rates calculated using Sphere [44] (black) and solvent-amide proton exchange rates measured using CLEANEX-PM experiment [39,43] on CP12red (red). The similarity between both values indicated that CP12red is intrinsically disordered. The signal intensity as a function of the spin-lock delay in the CLEANEX-PM experiments is shown in Figure S1. (**b**) Gibbs-free energy of CP12ox backbone amides derived from the measured solvent-amine proton exchange using CLEANEX-PM on oxidized versus reduced CP12 (refer to Material and Method for details), assuming that the exchange falls into the EX2 regime that is highly probable at this low pH. The measured rates of exchange for CP12ox amide at pH 7 and pH 6 are shown Figure S2. (**d**) Value of the slope of the temperature dependence of the proton chemical shift for CP12ox residues. The line at -4.6 ppm.K^{-1} indicates the threshold below which the data indicate the absence of hydrogen bond [50]. The temperature dependence curves of the chemical shift of the amine proton for all CP12ox residues are shown Figure S4. (**c**) Structure of the stable C-terminal helical turn with the amide protons protected from the exchange with water highlighted in red, and those exposed to exchange in green. (**e**) On the same structure, the amide proton for which the temperature dependence of the chemical shift has a positive slope highlighted in red.

3.2. Structural transition of the region encompassing the C23-C31 disulfide bridge upon oxidation of the isolated protein.

Contrary to the residues of the stable C-terminal region, most residues of the N-terminal region presented a kinetic of HN → H_2O exchange similar to the disordered reduced state (Figure 2b, Figure S1 and S2). Mass-spectrometry measurement of the proton-deuterium exchange on CP12ox also confirmed that these N-terminal amide protons exchange very quickly with the deuterated solvent (Figure S3). The variation of chemical shift according to the temperature for these resonances had all more negative gradients than -4.6.10^{-3} ppm.K^{-1} (Figure 2d), indicative of more labile protons [50] and this confirms the amide proton-exchange measurements. These data indicated that the N-terminal region surrounding the C_{23}-C_{31} disulfide bridge remains highly unstable.

The temperature dependence of the proton chemical shift is expected to be linear for a proton in a stable conformational state [51]. For a high number of amide protons in CP12ox the temperature dependence of the NMR frequency of amide proton of residues deviated from linearity, in particular those of neighboring the dynamic N-terminal region; for example the resonances assigned to residues A_5, V_{45} as well as a high field shifted glycine resonance that is putatively assigned to the single glycine of the N-terminal region G_{26} (Figure S4). This was also the case for several unassigned resonances,

Preprints (www.preprints.org) | NOT PEER-REVIEWED | Posted: 2 April 2021 doi:10.20944/preprints202104.0048.v1

that we have ascribed to the region L_{8}-A_{43} [31]. Of note, a few residues of the C-terminal turn also presented a non-linear temperature dependence of their amide proton chemical shift (L_{62}, E_{63}, A_{69}, A_{72}, R_{76}, Figure S4).

The curvature in the temperature dependence of the chemical shift indicates a chemical exchange between two forms or more for which the relative population varies with temperature [51]. In line with these observations, two resonances were observed for the side chain indole amide of the single tryptophan residue at position 35 (Figure 3). One of these two resonances overlaid with that of $CP12_{red}$ Trp-Hε (Figure 3a). The ^{1}H chemical shift of this resonance had a linear dependence with a negative slope of -3.3 10^{-3} ppm.K^{-1} (Figure 3c), which is close to the threshold for disordered amide [50]. To ensure that this resonance, assigned to unfolded Trp-Hε, did not rise from a fraction of reduced proteins, Cu^{2+} was added to the sample to fully oxidize the protein and then removed before NMR acquisition. The spectrum remained identical (Figure 3b), indicating that the unfolded Trp-Hε resonance belongs to $CP12_{ox}$. The chemical shift temperature dependence of the second resonance had a positive slope (+8 10^{-3} ppm.K^{-1}), indicative of folded conformation. Interestingly, the difference in frequency between these two resonances assigned to the same proton decreased at high temperature, and this relates to an increase in intensity (and decrease in linewidth) for the folded Trp-Hε resonance (Figure 3c, Figure S5). The difference in frequency also decreased at higher pH (Figure 3b), and the resulted resonances at pH 8 and 9 fell in a linear chemical shift pattern defined by the two above mentioned unfolded and folded Trp-Hε resonances [52,53]. This behavior is strongly indicative of a chemical exchange in the intermediate timescale (μs-100 ms) between a disordered and a folded conformation, that becomes faster at higher temperature and at higher pH [54].

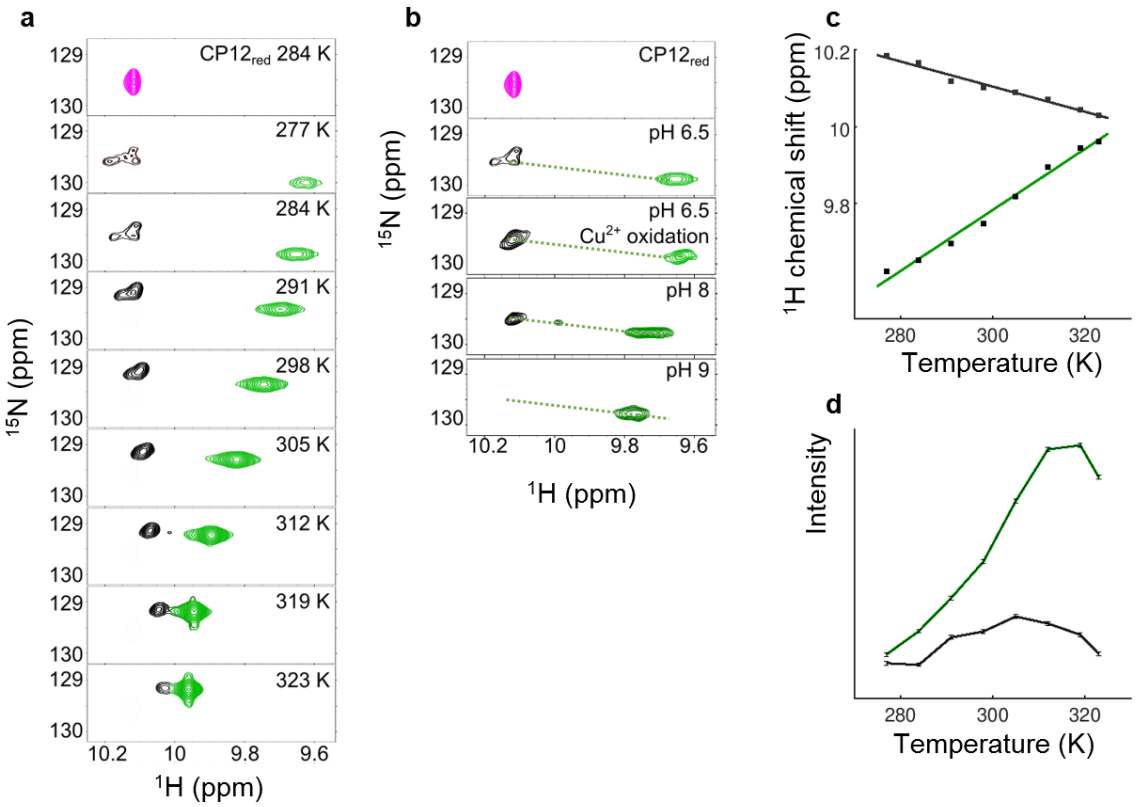

Figure 3: Temperature dependence of $CP12_{ox}$ Trp-ε resonances indicating a chemical exchange. (**a**) Series of ^{1}H-^{15}N spectra of $CP12_{ox}$ recorded at varying temperatures (277 K, 284 K, 291 K, 298 K, 305 K, 313 K, 319 K) and at pH 6.5 and plotted with the same contour levels. To ease the reading, the contour levels of each resonance are colored differentially. In (**a**) and (**b**), above the series, the spectrum of $CP12_{red}$ at 284 K is shown (magenta). (**b**) ^{1}H-^{15}N spectra of CP12 recorded at 284K at varying pH (pH 6.5 as in A, pH 8 and pH 9). An additional spectrum is shown at pH 6.5 where the

Preprints (www.preprints.org) | NOT PEER-REVIEWED | Posted: 2 April 2021 doi:10.20944/preprints202104.0048.v1

protein has been pre-treated with Cu^{2+} to ensure full oxidation. The paramagnetic ion was removed by dialysis before NMR acquisition. (**c**) Temperature dependence of the proton chemical shift for each of these $CP12_{ox}$ Trp-ε resonances using the same color coding (Figure S4). (**d**) Temperature dependence of the resonance intensity for each of these $CP12_{ox}$ Trp-ε resonances using the same color coding (refer to Figure S5).

3.3. Structural properties of $CP12_{red}$ in the presence of C.reinhardtii cell extract.

CP12 is located in a highly dense organelle, the chloroplast, and we aimed at grasping the effect of the presence of the macromolecules of its physiological environment on the structural states of CP12 in its reduced (light) and oxidized (dark) states. To mimic the chloroplast environment, we thus added crude cell extract at high concentration (15 to 19 mg.mL^{-1} of proteins) to purified ^{15}N-CP12 such that the observed CP12 proteins represent 2 to 3% of the total mass of protein. On the reduced and disordered protein, there was no significant chemical shift displacement, indicating that the protein remains in a disordered state (Figure 4b), with the exception of the last two resonances E_{79} and D_{80}. The resonances of the N-terminal residues up to K_{17} including the His-tag were broadened beyond detection compared to the isolated protein (Figure 4d). Other resonances were broadened in the presence of cell extract compared to the isolated protein: E_{40} and L_{41}, K_{48} and K_{49}, as well as few resonances of the C-terminal region (D_{70} to D_{72}, C_{75} and the last two residues E_{79}, D_{80}). On the contrary, the region C_{31}-A_{34} did not present any chemical shift variation, or specific line-broadening in the presence of cell extract. The translational diffusion coefficient at 4°C of reduced ^{15}N-CP12 in the presence of cell extract was less than 2 10^{-11} m^2.s^{-1} that is significantly lower compared to that of the isolated reduced protein (9.3 ± 0.15 10^{-11} m^2.s^{-1}, Figure S6).

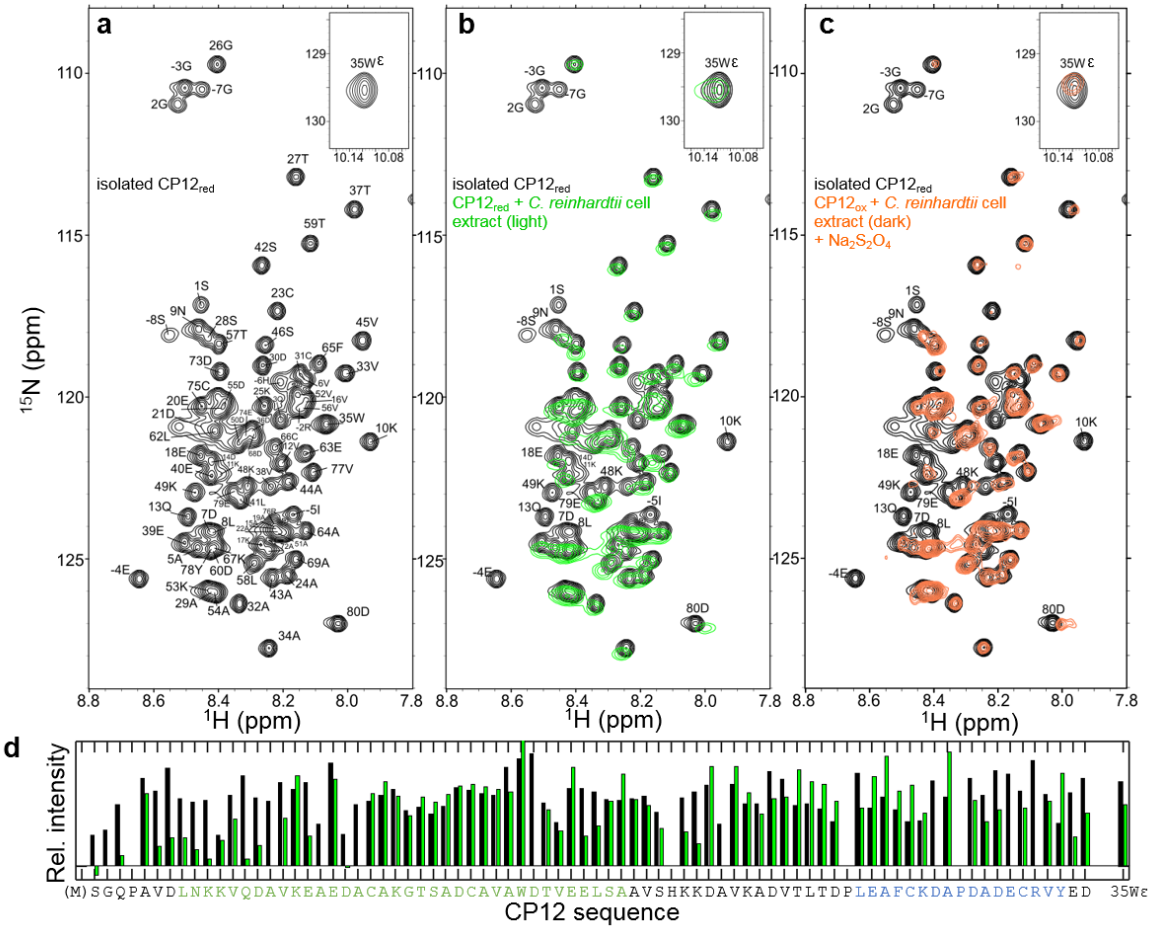

Figure 4: $CP12_{red}$ in isolation and in presence of *C. reinhardtii* cell extract. (**a**) ^{1}H-^{15}N HSQC spectrum of isolated $CP12_{red}$. The region of the tryptophan side-chain is shown in the insert. (**b**) overlay of the ^{1}H-^{15}N HSQC spectra of isolated $CP12_{red}$ (black) and that of CP12 in presence of *C. reinhardtii* cell extract (green, molecular crowding corresponding to 15 mg/mL of proteins). The data is recorded in

Preprints (www.preprints.org) | NOT PEER-REVIEWED | Posted: 2 April 2021 doi:10.20944/preprints202104.0048.v1

the presence of 20 mM DTT_{red}. (**c**) ^{1}H-^{15}N HSQC of CP12 in presence of *C. reinhardtii* cell extract collected in the dark (molecular crowding corresponding to 19 mg/mL of proteins), 0.1 mM DCMU and 20 mM dithionite as a strong reducing agent. (**d**) Signal intensities for all residues in the ^{1}H-^{15}N HSQC spectrum of isolated $CP12_{red}$ (black), and in the ^{1}H-^{15}N HSQC spectrum of $CP12_{red}$ in presence of *C. reinhardtii* cell extract (green). Signal intensities were normalized against the mean of all intensities.

3.4. Structural properties of the C_{66}-C_{75} disulfide bridge in $CP12_{ox}$ in the presence of C. reinhardtii cell extract.

The ^{1}H-^{15}N HSQC spectrum of oxidized and partially folded CP12 in the presence of cell extract also remarkably resembles that of the isolated protein (Figure 5b). As for $CP12_{red}$, the His-tag and the N-terminal residues (up to D_{14}) resonances were also broadened beyond detection in the presence of cell extract (Figure 5d). On the contrary, the C-terminal region (from K_{53} onwards) presented relatively narrow linewidths and identical chemical shift as compared to the isolated protein. The resonances for the residues A_{15} to S_{42} were broadened beyond detection both in the isolated protein and in the presence of cell extract. On the isolated protein, resonance linewidths were large up to residues S_{42} but in the presence of cell extract resonance linewidths were large for all residues until D_{50}. The translational diffusion coefficient at 4°C of oxidized ^{15}N-CP12 in the presence of cell extract was $4 \pm 0.5\ 10^{-11}\ m^2.s^{-1}$ that is significantly lower compared to that of the isolated oxidized protein ($9.8 \pm 0.2\ 10^{-11}\ m^2.s^{-1}$, Figure S6).

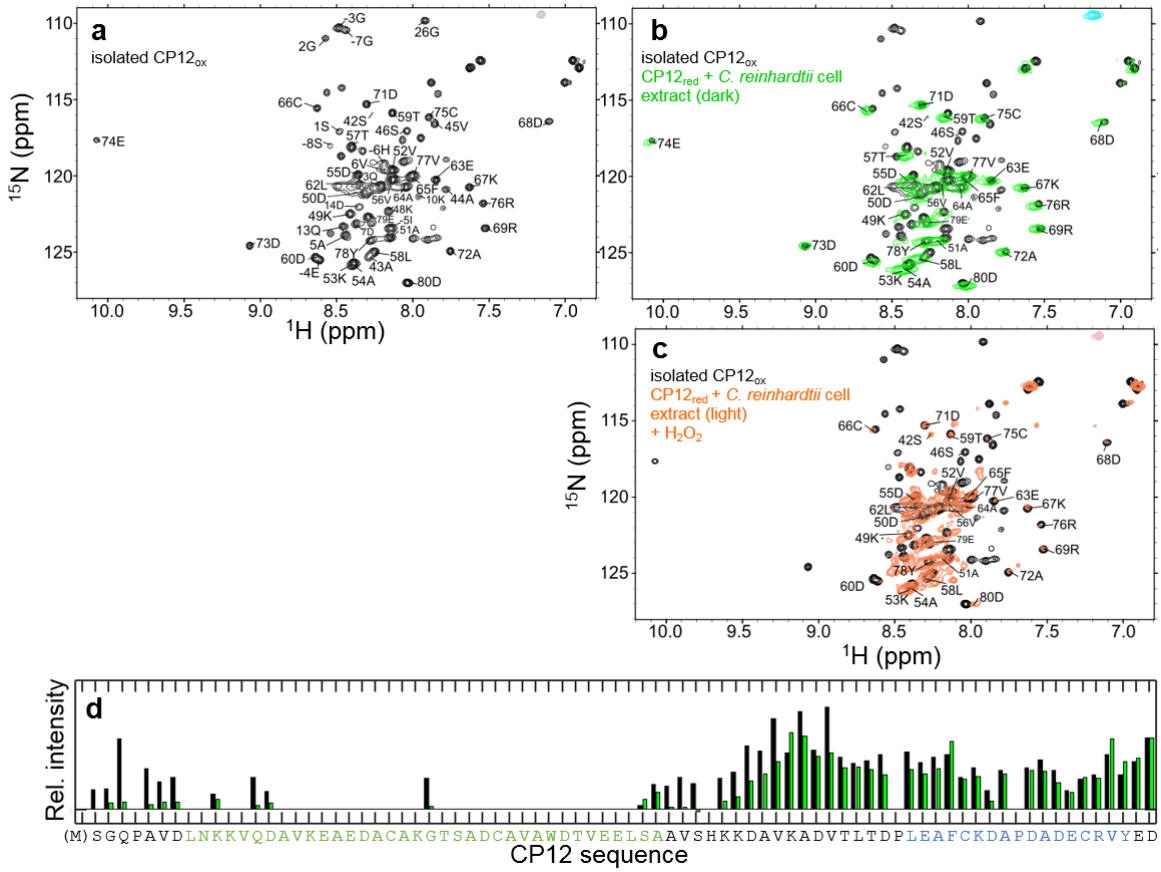

Figure 5: $CP12_{ox}$ in isolation and in presence of *C. reinhardtii* cell extract. (**a**) ^{1}H-^{15}N HSQC spectrum of isolated $CP12_{ox}$. (**b**) overlay of the ^{1}H-^{15}N HSQC spectra of isolated $CP12_{ox}$ (black) and that of CP12 in presence of *C. reinhardtii* cell extract (green, molecular crowding corresponding to 19 mg/mL of proteins). The data is recorded in the presence of 20 mM DTT_{ox}, and 0.1 mM DCMU. The assignments of the resonances that are observed in the presence of cell extract are indicated. (**c**) ^{1}H-^{15}N HSQC of CP12 in presence of *C. reinhardtii* cell extract collected in the light (molecular crowding corresponding to 15 mg/mL of proteins) and 20 mM H_2O_2 as a strong oxidizing agent. (**d**) Signal intensities for all

Preprints (www.preprints.org) | NOT PEER-REVIEWED | Posted: 2 April 2021 doi:10.20944/preprints202104.0048.v1

residues in the ^{1}H-^{15}N HSQC spectrum of isolated $CP12_{ox}$ (black), and in the ^{1}H-^{15}N HSQC spectrum of $CP12_{ox}$ in presence of *C. reinhardtii* cell extract (green). The signal intensities are normalized against the mean of all intensities.

3.5. Thermodynamical properties of the redox transition of both disulfide bridges in isolated CP12.

CP12 is a CDP, and its function is related to the significant structural transition upon reduction or oxidation of the two cysteine residues pair. From the above results, we showed that the two disulfide bridges are located into two structurally distinguishable regions separated by a flexible linker. We monitored the thermodynamical properties of these two disulfide bridges using a titration with the redox mediator DTT_{ox}/DTT_{red} [45,55] on isolated CP12. Surprisingly, the use of the well-known redox mediator GSSG/GSH was not possible because the redox transition was not reversible with this mediator [45]. The standard redox mid-potentials at pH 7.0 were -284 mV for the C_{23}-C_{31} cysteine pair (Figure 6a) and -291 mV for the C_{66}-C_{75} pair (Figure 6b). The variation of the standard redox mid-potential of the N-terminal pair followed the expected pH-dependence for a disulfide bridge (-59.1 mV per pH unit [45], Figure 6a). On the contrary, the redox mid-potential measured at pH 8 for the C-terminal disulfide bridge was more negative than expected (Figure 6c), indicating a possible pH-induced stability for the C-terminal folded oxidized state.

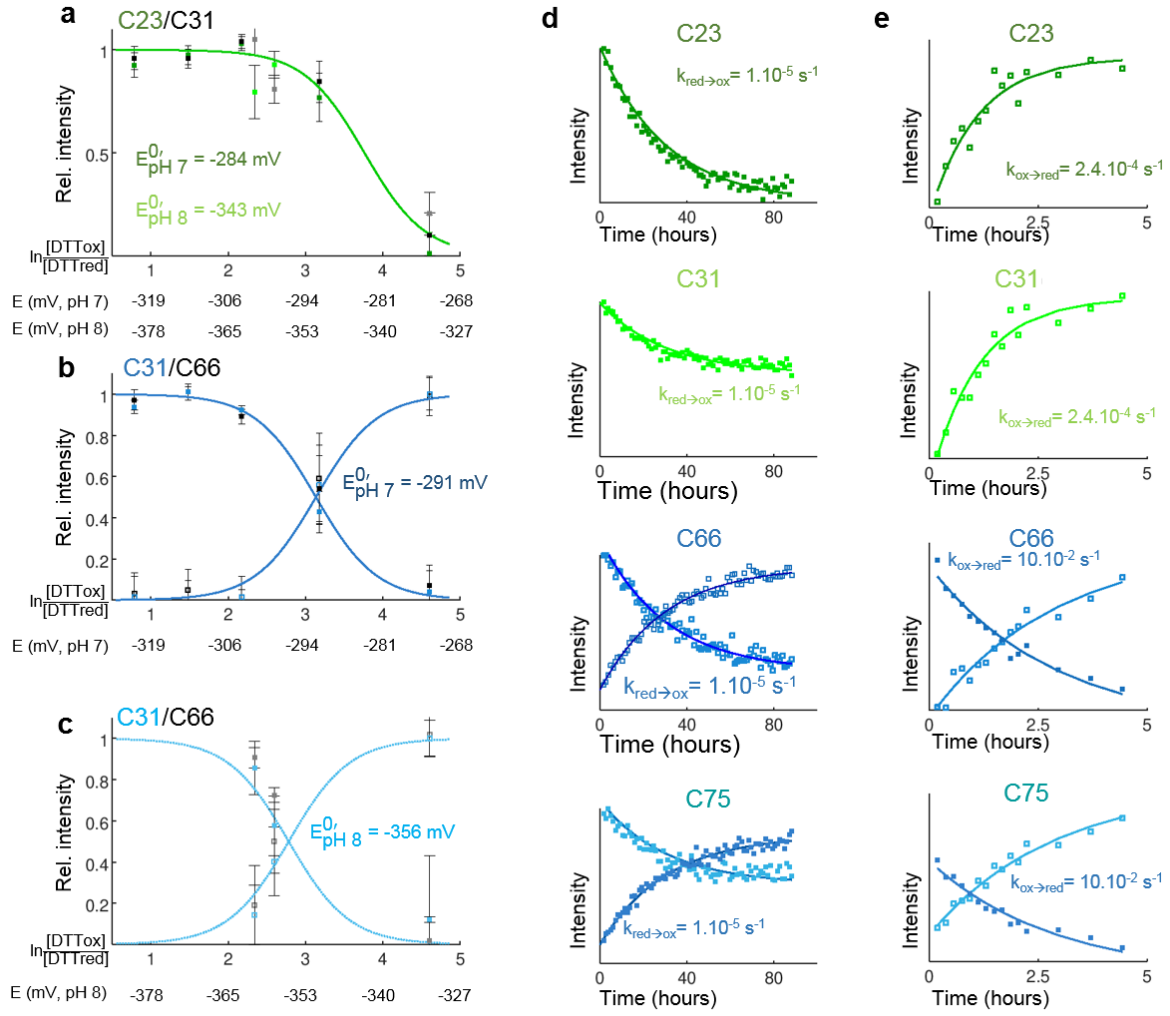

Figure 6: Redox transition of isolated CP12. (**a**) Thermodynamic of the redox transition for the N-terminal disulfide bridge. Signal intensities at NMR frequencies of reduced cysteine residues C_{23} (dark

Preprints (www.preprints.org) | NOT PEER-REVIEWED | Posted: 2 April 2021 doi:10.20944/preprints202104.0048.v1

and light green) and C_{31} (grey and black), plotted as a function of the logarithm of the measured [DTT_{ox}] / [DTT_{red}] ratio (refer to Material and Methods section). The corresponding electropotential at pH 7 or pH 8 are indicated below. The redox titration was performed at pH 7 (dark green and black) and pH 8 (light green and grey). (**a**) Thermodynamic of the redox transition for the N-terminal disulfide bridge measured at pH 7. Signal intensities at NMR frequencies of reduced (filled squares) and oxidized (open squares) cysteine residues C_{66} (dark blue) and C_{75} (black), plotted as a function of logarithm of the measured [DTT_{ox}] / [DTT_{red}] ratio (refer to Material and Methods section). The corresponding electropotential at pH 7 is indicated below. (**c**) Same as B at pH 8. The color coding is light blue for C_{66} and grey for C_{75}. The redox mid-potential of the C_{66}-C_{75} disulfide bridges at pH 8 is more different that that at pH 7 than the expected -59.1 mV difference per pH unit. (**d**) Real-time monitoring of the oxidation. Signal intensity as function of time after buffer exchange in air-oxidized at NMR frequency of reduced C_{23} (top), reduced C_{31} (below), reduced and oxidized C_{66} (below, open and filled square respectively) and reduced and oxidized C_{75} (bottom, open and filled square respectively). The fits using the equations $I/I_0 = e^{-k_{red\rightarrow ox}t}+c$ and $I/I_0 = c-e^{-k_{red\rightarrow ox}t}$ are shown, where c is a constant, k is the rate constant of the oxidation cysteine residues. The real time monitoring of the oxidation for all CP12 residues is shown Figure S7. (**e**) Real-time monitoring of the reduction. The color coding is the same as above. The fits using the equations $I/I_0 = e^{-k_{ox\rightarrow red}t}+c$ and $I/I_0 = c-e^{-k_{ox\rightarrow red}t}$ are shown, where c is a constant, k is the rate constant of the transition from oxidized to reduced cysteine residues. The reduction rate for all CP12 residues is shown in Figure S8.

3.6. Rate of oxidation and reduction of both disulfide bridges in isolated CP12, probed by real-time NMR.

Using NMR spectroscopy, we followed the oxidation or reduction in real-time of each disulfide bridge of isolated CP12 upon changing the redox potential of the solution by buffer exchange into air-aerobic buffer or upon addition of 20 mM DTT_{red}. The rates of the oxidation for both disulfide bridges were identical, indicating their synchronisation (Figure 6d, Figure S7). On the contrary, the reduction of the N-terminal bridge was much faster than that of the C-terminal bridge, indicating asynchrony in their reduction (Figure 6e, Figure S8). These rates measured on the isolated protein are not representative of those in the cell, where redox transitions are catalyzed by the complex Trx network but reflect the structural stability of both regions encompassing the two respective disulfide bridges.

3.7. Reversible redox transition of CP12 in the presence of C. reinhardtii cell-extract probed by real-time NMR.

Upon addition of crude cell extract from cells exposed to 24 hours of dark, the ^{15}N-$CP12_{ox}$ protein was highly unstable, and its ^{1}H-^{15}N spectrum was quickly converted and overlaid that of $CP12_{red}$ within 20-40 min, even when 20 mM DTT_{ox} was added. This indicates that the electron transfer of the photosynthesis was active in these crude cell extract and can activate the Trx network resulting in the reduction of DTT and CP12 when cells were transferred from dark to the spectrometer. We therefore added 0.1 mM DCMU that inhibits photosystems II and electron transfer reactions, and this prevented CP12 reduction.

We monitored in real time the redox transition triggered by strong reducing or oxidizing agents (in the presence of PSII inhibitor not to interfere with the Trx network). When dark extracts were exposed to strong reducing conditions (20mM $Na_2S_2O_2$), the ^{1}H-^{15}N spectrum of the protein was quickly converted and overlaid that of $CP12_{red}$ (Figure 4c). Reciprocally, when light extracts were exposed to oxidizing conditions (20mM H_2O_2) the ^{1}H-^{15}N spectrum of the protein was quickly converted within 20 min and overlaid that of $CP12_{ox}$ (Figure 5c). Altogether, these results show that both oxidized-to-reduced and reduced-to-oxidized transitions of CP12 are very fast in *C. reinhardtii* cell extract, contrary to isolated CP12, very likely thanks to the presence of TRXs in the extracts.

4. Discussion

CP12 is present in the chloroplast of photosynthetic organisms from cyanobacteria, green algae and plants, red algae as well as heterokonts [27,28,32]. Various functions have been assigned to this

Preprints (www.preprints.org) | NOT PEER-REVIEWED | Posted: 2 April 2021 doi:10.20944/preprints202104.0048.v1

protein, in particular the dark-down regulation of two CBB enzymes: GAPDH and PRK, as well as their fast re-activation upon dark-to-light transition [22]. Besides, genetic and proteomic studies on higher plants and heterokonts report results that suggest that CP12 has other functions, for example related to stress regulation [32,56–59]. The enigmatic and multiple functions of CP12 is not an unusual property for a protein belonging to the CDP family [1]. In this study, we report on the structural transition of CP12 at the molecular level occurring upon change in redox potential, which is the basis for its proposed regulatory functions.

4.1. Isolated CP12$_{red}$ is intrinsically disordered

In the light, the photosystems I and II impose a strong reducing potential that is mediated to the chloroplastic proteins via the Fdx-dependent Trx [60], and this network is probably the best studied within the chloroplast [61]. Under reducing conditions, we recorded the amide protons exchange rate with solvent by NMR and mass spectrometry for the purified CP12 and these data confirmed that the unfolded reduced state of CP12 is highly flexible (Figure 2a), as we have described previously by SAXS and NMR spin-relaxation experiments [30,31]. The absence of pre-formed motif is also confirmed in this study by the homogeneous NMR resonance intensity for all CP12$_{red}$ residues (Figure 4d). Indeed, the existence of a small proportion of pre-formed motifs would give rise to selective broadening of the NMR resonances [30,62]. Together, these data confirm that CP12$_{red}$ is intrinsically disordered (Figure 7a).

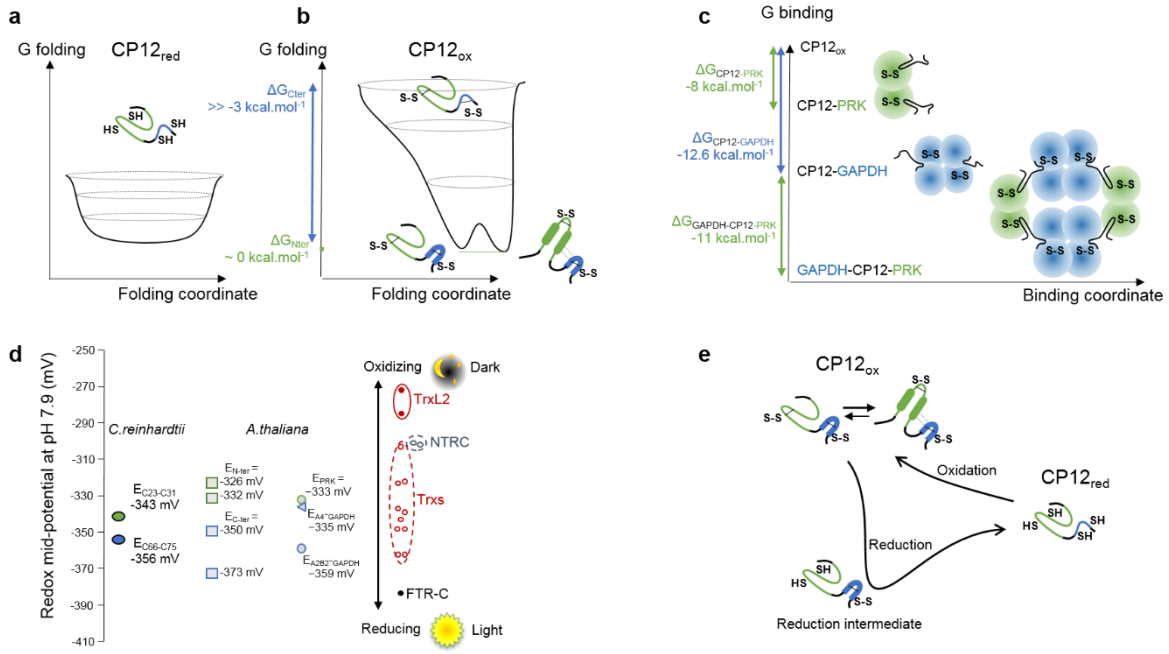

Figure 7: Overview of the thermodynamic equilibria of CP12. (**a**) Gibbs free energy of folding for CP12$_{red}$. (**b**) Gibbs free energy of folding for CP12$_{ox}$. (**c**) Gibbs free energy of binding for CP12$_{ox}$. (**d**) The midpoint redox potentials for the CP12 C-terminal disulfide bridge (blue filled circle) and N-terminal disulfide bridge (green filled circle) measured in this study are compared to the midpoint potential for *A. thaliana* CP12 isoforms (blue and green squares), as well as for A_2B_2-GAPDH, A_4-GAPDH and PRK activity as determined in [63–65] (blue open triangle, blue open circle and green open circle respectively). For comparison, the redox potential of the ferredoxin-Trx reductase C-subunit (FTR-C) is shown in black, that of the NADPH-Trx reductase C (NTRC) in open blue circles, various Trx isoforms in red, as well as that of the Trx like 2 (TrxL2), as in Yoshida et al[66]. (**e**) Kinetics of the oxidation (right to left) and reduction (left to right) highlighting the synchrony of the first, and the existence of a reduction intermediate for the second.

4.2 The two disulfide bridges are in regions with distinct structural properties in isolated CP12$_{ox}$.

Preprints (www.preprints.org) | NOT PEER-REVIEWED | Posted: 2 April 2021 doi:10.20944/preprints202104.0048.v1

In the dark, oxidizing conditions prevail in the chloroplast [61], principally because the source of electron (water splitting) does not fuel the Fdx-dependent Trx system. Oxidation of chloroplast proteins is then catalyzed by both the Fdx-dependent and the NADPH-dependent Trx systems. In the case of CP12, the four cysteine residues form two disulfide bridges. Our results showed that the C-terminal disulfide bridge (C_{66}-C_{75}) is located in a region in which amide proton are highly protected against solvent exchange (Figure 2b). This confirms that this region encompassing residues L62-Y78 is highly stable, as we have previously shown by NMR spin-relaxation measurements [31] (Figure 7b). The N-terminal disulfide bridge (C_{23}-C_{31}) is in a region that remains highly dynamic, as shown here by the absence of protection against amide proton exchange by NMR and MS (Figure 2b, Figure S3). As shown previously for *C. reinhardtii* and *A. thaliana* CP12 proteins, the residues of this long N-terminal region encompassing residues L8-A44 gives rise to broad NMR resonances [29,31]. We used the resonances from the unique tryptophan side chain to probe for the origin of this line broadening. Two resonances are observed (Figure 3). One resonance that is the most down field overlays with that of the same proton in $CP12_{red}$. Its variation with temperature follows what is expected for a residue in a disordered region [50,51]. Also, this resonance is not observed at pH 9, and this is also indicative of fast amide proton exchange with water, and therefore absence of structure [67]. The second resonance is always observed even at high pH, and varies with temperature with a positive slope, that is indicative of hydrogen bond (Figure 3) [50,51]. Together, these data confirm our previous SAXS analysis that suggested that the N-terminal region can be either disordered or folded [31]. When oxidizing conditions prevail in the chloroplast, the pH in the stroma decreases to pH 7 [68]. Such a drop in pH induced a displacement of the resonances arising from Trp-Hε within a linear chemical shift pattern defined by the above mentioned two resonances with a larger difference in intensity (Figure 3b). This displacement is accompanied by a decrease in linewidth and an increase in signal intensity. This indicates that the speed of interconversion between the two states is modified at high pH, and becomes slower in NMR intermediate exchange timescale (μs-ms) [52,53,69], as we have previously suggested based on NMR spin relaxation experiments [31].

Altogether, these data suggest that in its oxidized state, CP12 is in an atypical conformational ensemble, in which the C-terminal region (L_{62}-Y_{78}) is highly stable, whereas the N-terminal region (L_8-A_{44}) co-exists in a folded and unfolded states in exchange in the ms timescale (Figure 7b). In other word, the C-terminal region of CP12 undergoes a complete disorder-to-order transition upon increasing the redox potential, as described for several redox-dependent CDP [3]. On the contrary, the N-terminal region is not fully ordered in the oxidized state. For this region, the folded state is only partially stabilized under oxidizing condition. Our previous SAXS analysis suggested relative population for the disordered and ordered conformation of 40%:60%, and our current temperature and pH dependent analysis suggest that this equilibrium is strongly dependent on the physico-chemical conditions (Figure 7b). These two regions (folded C-terminal helical turn and highly dynamic N-terminal region) are separated by a flexible linker of ten residues (D_{50}-D_{60}) that also delimits two regions of interaction with different partners.

4.3. The distinct regions of $CP12_{ox}$ differ in structural dynamic and in affinity for their interacting partners.

$CP12_{ox}$ associates and inhibits PRK and GAPDH in a ternary complex [23]. The structure of this complex has been solved recently for proteins from *A. thaliana* [26] and from the cyanobacterium *Thermosynechococcus elongatus* [25]. In these structures, the C-terminal region of $CP12_{ox}$ folds into a helical turn that is identical to the stable structure that we have computed from NMR data [31]. The very high affinity for the C-terminal region of CP12 for GAPDH (sub nM) relates to a low delta Gibbs-free energy of -12.7 $kcal.mol^{-1}$, a value that is below the mean value for complexes between two ordered proteins from ~200 studies [70] (Figure 7c). On the contrary, the N-terminal region has a much lower affinity for PRK (-1.3 μM) [23], that relates to a higher delta Gibbs-free energy of -8 $kcal.mol^{-1}$. This value of delta Gibbs free energy is identical to the mean value for complexes between an ordered and a disordered protein [70]. The $CP12_{ox}$ binding region with PRK is located in the unstable and highly dynamic N-terminal region [24]. In line with the above described structural dynamic for this region in the isolated protein, in the crystal structure of the PRK-CP12-GAPDH from

Preprints (www.preprints.org) | NOT PEER-REVIEWED | Posted: 2 April 2021 doi:10.20944/preprints202104.0048.v1

A. thaliana [26] and in the cryo-EM structure from *T. elongatus* [25], the least resolved regions are the interaction surface between CP12 and PRK. Altogether, the interface between Nter-CP12$_{ox}$ and PRK seems to be highly dynamic contrary to the Cter-CP12$_{ox}$ interface with GAPDH, and these can be related to the relative structural stability of these two regions.

The two structurally and functionally distinguishable regions of CP12 - a stable C-terminal helical turn and an unstable N-terminal region - fused via a flexible linker offer a complex and tightly controlled mean to regulate the two binding partners. Interestingly, photosynthetic organisms possess CP12 homologs where only the C-terminal region ($C_{66}xxxP_{70}xxxC_{75}$) is fused to other enzymes such as GAPDH-B isoforms [71] or adenylate kinase, ADK3 [72,73]. These proteins also bind to GAPDH with a high affinity. Besides, other organisms possess CP12 homologs with the conserved N-terminal motif $A_{34}WxxVEEL_{41}$ that is embedded in the dynamical PRK-binding region defined above [27,32], and the function of these proteins remains to be elucidated.

4.4. Thermodynamically independent and reversible redox transition of both disulfide bridges in CP12.

As mentioned above, the principal known function for CP12 is the redox regulation of CBB enzymes in the chloroplast. Here, we report on redox titrations by NMR that demonstrated that the four conserved cysteine residues of CP12 from *C. reinhardtii* could form two intermolecular disulfide bridges with different redox mid-potentials (Figure 7d). The redox mid-potential for the C_{23}-C_{31} cysteine residues pair ($E^0_{pH\,8\ C.r\,N\text{-}ter}$ = –343 mV) is more negative than those measured for the N-terminal disulfide bridge of *A. thaliana* CP12 isoforms ($E^0_{pH\,7.9\ A.t\,N\text{-}ter}$ = −326mV in the two isoforms CP12-1 and CP12-2 and $E^0_{pH\,7.9\ A.t\,N\text{-}ter}$ = −332mV in the isoform CP12-3 [65]), analyzed from redox titrations using 5,5′-dithiobis(2-nitrobenzoic acid) to detect thiol groups. The redox mid-potential for the *C. reinhardtii* C-terminal disulfide ($E^0_{pH\,8\ C.r\,C\text{-}ter}$ −356 mV) is an intermediate with that found for the isoforms CP12-1 & CP12-2 of *A. thaliana* ($E^0_{pH\,7.9\ A.t\,C\text{-}ter}$ = -350mV) and that found for the isoform CP12-3 ($E^0_{pH\,7.9\ A.t\,C\text{-}ter}$ = -373mV) [65]. These more negative values in the alga CP12 redox mid-points are in contradiction with the previous observation that the redox potential of Trxs in the alga are less negative than higher plant counterpart [74]. The different technique might also be responsible for the difference. Above all, and similarly with what has been observed for *A. thaliana*, our results indicate that the N terminal disulfide in *C. reinhardtii* requires less reducing conditions than the C-terminal disulfide, i.e. in thermodynamic terms, the N-terminal disulfide is easier to reduce than the C terminal disulfide.

During light to dark transition, partially oxidizing conditions would cause the formation of the C-terminal disulfide of CP12 ($E^0_{pH\,8}$ = –358 mV) and then favour the formation of the binary complex A_4-GAPDH-CP12 (Figure 7c & d). At these electropotential values, the A_4-GAPDH tetramer from *A. thaliana* ($E^0_{pH\,7.9\ A4\text{-}GAPDH}$ = -335 mV) is still reduced, but the A_2B_2-GAPDH tetramer -that contains a CP12 homolog extension is also getting oxidized ($E^0_{pH\,7.9\ A2B2\text{-}GAPDH}$ = -359 mV) [64]. The redox mid-potential of CP12 C-terminal bridge is consistent with the hypothesis proposed in [17] that CP12 is a redox mediator for GAPDH regulation. By approaching darkness, further oxidation of Trxs would lead to the formation of N-terminal disulfide formation in CP12 ($E^0_{pH\,8\ N\text{-}ter}$ = –343mV) allowing the PRK-CP12-GAPDH formation, and finally the regulatory disulfide in PRK is able to form ($E^0_{pH\,7.9\ PRK}$ = –333 mV) [63]. These results provide key insights to understanding the biological assembly and the regulation of this ternary complex.

4.5. Asynchrony of the reduction of the two disulfide bridges, synchrony of their formation

From a kinetic point of view, the rates of oxidation of the cysteine residues at the N and C terminal extremities were similar, which validates the above discussion on equilibrium. On the contrary, the rates of reduction were different (Figure 7E). The synchrony of oxidation can be explained by the fully disordered nature of the reduced form. Similarly, the asynchrony of reduction can be explained by the dual nature of CP12$_{ox}$ with a very dynamic N terminal end, being prone to fast reduction, and a stable C terminal helical turn less prone to reduction. On the isolated CP12, these processes, oxidation and reduction, were slow. In contrast, *in-situ* - that is in CP12 physiological

Preprints (www.preprints.org) | NOT PEER-REVIEWED | Posted: 2 April 2021 doi:10.20944/preprints202104.0048.v1

environment with active cellular redox-mediators - the redox transitions were much faster [17]. It would be interesting to compare the rate of thiol reduction in the cell (kinetic of CP12 thiol to disulfide transition) with the rate of reduction of the electropotential in the chloroplast upon dark to light transition [15], as this could provide a further fine regulation mean for CBB enzyme activity.

4.6. Effect of cell extract on N_{ter}-CP12 and C_{ter}-CP12

Within the chloroplast, redox modulation is clearly open to modification by a number of other parameters such as stromal pH, Mg^{2+} and metabolite concentrations, and above all, crowding. The chloroplast contains numerous phases including starch granules, thylakoid membranes [75], pyrenoid (the liquid non-membranous compartment containing the ribulose-1,5-bisphosphate carboxylase oxygenase) [76,77] as well as natural deep eutectic molecules with an extremely high local concentration [78–80]. The physico-chemical conditions prevailing in the chloroplast stroma therefore have to be taken into account when trying to unravel the processes of protein folding. CP12 is known to exist in chloroplast of in *A. thaliana* both in light and dark conditions [81], we thus aimed at characterizing the effect of the chloroplast environment on both $CP12_{red}$ and $CP12_{ox}$. In order to approach the physico-chemical condition that CP12 encounters in the chloroplast, we added *C. reinhardtii* cell extract to purified ^{15}N-CP12. The cytoplasm of *C. reinhardtii* is very limited in volume compared to other eukaryotic cells [82], such that chloroplast molecules contribute to a major fraction of the cell extract. Besides, the interaction network of CP12 is expected to be present in cell extract as it has been previously shown that sonication does not break the networks of interactions between partners [83].

We observed the structural state of CP12 in a large excess of *C. reinhardtii* cell extract (2 to 3% of protein are ^{15}N-CP12 in a total protein concentration of 15 to 19 mg.mL^{-1}). We observed that $CP12_{red}$ in-situ remains disordered, with a few residues being affected. Some residues present specific line broadening of their NMR resonances (for example the N-terminal residues, E_{40}-L_{41}, K_{48}-K_{49}), and this could be ascribed to specific binding of molecule with $CP12_{red}$. In the literature, no binding partners for $CP12_{red}$ have been identified, and this could be because their affinity are probably weak as this is often the case for disordered proteins [70]. These affinities might be increased in-situ, giving rise to the observed line-broadening. Indeed, molecular crowding is known to increase the equilibrium constants of association events [84,85]. For example, the association equilibrium constant for the dimerization of a 40-kDa monomer is 8 to 40-fold higher if the protein is in *E. coli* cytoplasm, where the concentration of proteins is extremely high (200 to 320 mg/mL), compared to the same phenomenon in an aqueous solution [86].

In the presence of oxidized cell extract, only the stable C-terminal helical turn is observed in the NMR spectrum (Figure 5). This could be because the region concerned with line broadening ascribed to the millisecond-timescale equilibrium on the isolated protein (L_9-A_{43}) is expanding in the presence of cell extract (N-terminal to D_{50}). $CP12_{ox}$ thus behaves like many proteins that were shown to be more thermodynamically stable in the presence of crowding agents because of excluded-volume effects and higher chances of intra-molecular interactions [87]. Another origin for line broadening could be the association within a macro-molecular complex as discussed above for $CP12_{red}$.

The translational diffusions of both $CP12_{ox}$ and $CP12_{red}$ are also dampened by the presence of *C. reinhardtii* cell extract (Figure S6) and are reduced by a factor of two for $CP12_{ox}$ and by more than 5 for $CP12_{red}$. The macromolecular concentration in our experiment was 15 to 19 mg/mL of protein, and an increase in viscosity is thus expected. Ordered proteins are expected to be more affected by the increase in viscosity than disordered protein [88,89], but this is not the case for the partially folded $CP12_{ox}$ that is less affected than the disordered $CP12_{red}$. A succession of association-dissociation events with several chloroplast partners can also explain this very slow diffusion. The presence of broadened resonances in both spectra as discussed above indicates the presence of such association-dissociation events. Surprisingly, diffusion of $CP12_{red}$ is more affected than $CP12_{ox}$, and this may suggest a higher number of weak (specific or not) interaction events for the disordered reduced state.

Authors should discuss the results and how they can be interpreted in perspective of previous studies and of the working hypotheses. The findings and their implications should be discussed in the broadest context possible. Future research directions may also be highlighted.

5. Conclusions

We have shown here that CP12 can regulate association/dissociation with two of its known partners via a range of equilibria: a folding equilibrium that is modulated according to redox-potential, pH and temperature, as well as two binding equilibria. Because these regulatory processes respond to subtle change in the physico-chemical conditions of the CP12 environment, it is important to report on these in-situ. Performing in-cell NMR would be ideal, as this has been done for bacteria, yeast, oocyte and mammalian cells [90], but it has remained a real challenge for photosynthetic cells [91]. The main question remains: where is CP12 in the chloroplast? Proteins spatial organization in *C. reinhardtii* chloroplasts have been described by Mackinder et al [75,92] but these studies had not allowed to localize the enigmatic CP12 proteins. Moreover, to complete our preliminary attempt to reconstitute the chloroplast environment, further investigations are required to understand the structural mechanisms that promote highly regulated unfolding-folding transitions under specific physiological conditions, including not only redox but pH, temperature, metabolites to finely tune the photosynthetic metabolism.

Supplementary Materials: The following are available online at www.mdpi.com/xxx/s1, Figure S1: Amide proton exchange NMR data, Figure S2: Solvent-amide proton exchange rates, Figure S3: Amide proton exchange with deuterium probed by mass spectrometry, Figure S4: Temperature dependence of the proton chemical shift for $CP12_{ox}$ resonances, Figure S5: Temperature dependence of the signal intensity for $CP12_{ox}$ resonances, Figure S6: Hydrodynamics of $CP12_{ox}$ and $CP12_{red}$ measured by DOSY-NMR, Figure S7: Real-time monitoring of the oxidation for all CP12 residues, Figure S8: Real-time monitoring of the reduction for all CP12 residues.

Author Contributions: Conceptualization, Helene Launay and Brigitte Gontero; Investigation, Helene Launay, Hui Shao, Olivier Bornet, Francois-Xavier Cantrelle and Regine Lebrun; Methodology, Olivier Bornet, Francois-Xavier Cantrelle and Regine Lebrun; Resources, Hui Shao, Olivier Bornet, Francois-Xavier Cantrelle and Regine Lebrun; Supervision, Helene Launay and Brigitte Gontero; Validation, Helene Launay, Veronique Receveur-Brechot and Brigitte Gontero; Writing – original draft, Helene Launay and Brigitte Gontero; Writing – review & editing, Helene Launay, Regine Lebrun, Veronique Receveur-Brechot and Brigitte Gontero.

Funding: This research was funded by A*MIDEX, grant number AAP-IM2B-NE-2020-02-Launay. Financial support from the TGIR-RMN-THC Fr3050 CNRS is gratefully acknowledged. This work is supported by the CNRS. HS scholarship was founded by the Chinese Scholarship Council (201704910795).

Acknowledgments: We would like to thank Remy Puppo and Mathilda Daguze for experimental help. Financial support from the TGIR-RMN-THC Fr3050 CNRS is gratefully acknowledged. We would like to thank Dr Christopher Waudby, Pr Lewis Kay and Dr Enrico Rennella for sharing their NMR pulse sequences. We would like to thank Dr Frederic Carriere for inspiring and fruitful discussions.

Conflicts of Interest: The authors declare no conflict of interest.

References

1. Jakob, U.; Kriwacki, R.; Uversky, V.N. Conditionally and Transiently Disordered Proteins: Awakening Cryptic Disorder to Regulate Protein Function. *Chem. Rev.* **2014**, *114*, 6779–6805, doi:10.1021/cr400459c.
2. Smith, L.M.; Kelleher, N.L. Proteoform: A Single Term Describing Protein Complexity. *Nature Methods* **2013**, *10*, 186–187, doi:10.1038/nmeth.2369.
3. Reichmann, D.; Jakob, U. The Roles of Conditional Disorder in Redox Proteins. *Curr. Opin. Struct. Biol.* **2013**, *23*, 436–442, doi:10.1016/j.sbi.2013.02.006.
4. Ilbert, M.; Horst, J.; Ahrens, S.; Winter, J.; Graf, P.C.F.; Lilie, H.; Jakob, U. The Redox-Switch Domain of Hsp33 Functions as Dual Stress Sensor. *Nat. Struct. Mol. Biol.* **2007**, *14*, 556–563, doi:10.1038/nsmb1244.

5. Winter, J.; Ilbert, M.; Graf, P.C.F.; Ozcelik, D.; Jakob, U. Bleach Activates a Redox-Regulated Chaperone by Oxidative Protein Unfolding. *Cell* **2008**, *135*, 691–701, doi:10.1016/j.cell.2008.09.024.
6. Banci, L.; Bertini, I.; Ciofi-Baffoni, S.; Tokatlidis, K. The Coiled Coil-Helix-Coiled Coil-Helix Proteins May Be Redox Proteins. *FEBS Letters* **2009**, *583*, 1699–1702, doi:10.1016/j.febslet.2009.03.061.
7. Fraga, H.; Pujols, J.; Gil-Garcia, M.; Roque, A.; Bernardo-Seisdedos, G.; Santambrogio, C.; Bech-Serra, J.-J.; Canals, F.; Bernadó, P.; Grandori, R.; et al. Disulfide Driven Folding for a Conditionally Disordered Protein. *Sci Rep* **2017**, *7*, 16994, doi:10.1038/s41598-017-17259-4.
8. Holmgren, A. Thioredoxin. *Annu Rev Biochem* **1985**, *54*, 237–271, doi:10.1146/annurev.bi.54.070185.001321.
9. Michelet, L.; Zaffagnini, M.; Morisse, S.; Sparla, F.; Pérez-Pérez, M.E.; Francia, F.; Danon, A.; Marchand, C.H.; Fermani, S.; Trost, P.; et al. Redox Regulation of the Calvin-Benson Cycle: Something Old, Something New. *Front Plant Sci* **2013**, *4*, 470, doi:10.3389/fpls.2013.00470.
10. Zaffagnini, M.; Fermani, S.; Marchand, C.H.; Costa, A.; Sparla, F.; Rouhier, N.; Geigenberger, P.; Lemaire, S.D.; Trost, P. Redox Homeostasis in Photosynthetic Organisms: Novel and Established Thiol-Based Molecular Mechanisms. *Antioxid Redox Signal* **2019**, *31*, 155–210, doi:10.1089/ars.2018.7617.
11. Scheibe, R.; Anderson, L.E. Dark Modulation of NADP-Dependent Malate Dehydrogenase and Glucose-6-Phosphate Dehydrogenase in the Chloroplast. *Biochim Biophys Acta* **1981**, *636*, 58–64, doi:10.1016/0005-2728(81)90075-x.
12. Scheibe, R.; Geissler, A.; Fickenscher, K. Chloroplast Glucose-6-Phosphate Dehydrogenase: Km Shift upon Light Modulation and Reduction. *Arch Biochem Biophys* **1989**, *274*, 290–297, doi:10.1016/0003-9861(89)90441-4.
13. Kachru, R.B.; Anderson, L.E. Inactivation of Pea Leaf Phosphofructokinase by Light and Dithiothreitol. *Plant Physiol* **1975**, *55*, 199–202, doi:10.1104/pp.55.2.199.
14. Yoshida, K.; Hisabori, T. Biochemical Basis for Redox Regulation of Chloroplast-Localized Phosphofructokinase from *Arabidopsis Thaliana*. *Plant Cell Physiol* **2021**, doi:10.1093/pcp/pcaa174.
15. Cejudo, F.J.; Ojeda, V.; Delgado-Requerey, V.; González, M.; Pérez-Ruiz, J.M. Chloroplast Redox Regulatory Mechanisms in Plant Adaptation to Light and Darkness. *Front Plant Sci* **2019**, *10*, doi:10.3389/fpls.2019.00380.
16. Avilan, L.; Lebreton, S.; Gontero, B. Thioredoxin Activation of Phosphoribulokinase in a Bi-Enzyme Complex from *Chlamydomonas Reinhardtii* Chloroplasts. *J. Biol. Chem.* **2000**, *275*, 9447–9451, doi:10.1074/jbc.275.13.9447.
17. Knuesting, J.; Scheibe, R. Small Molecules Govern Thiol Redox Switches. *Trends Plant Sci.* **2018**, *23*, 769–782, doi:10.1016/j.tplants.2018.06.007.
18. Leegood, R.C.; Walker, D.A. Regulation of Fructose-1,6-Bisphosphatase Activity in Intact Chloroplasts. Studies of the Mechanism of Inactivation. *Biochimica et Biophysica Acta (BBA) - Bioenergetics* **1980**, *593*, 362–370, doi:10.1016/0005-2728(80)90073-0.
19. Vaseghi, M.-J.; Chibani, K.; Telman, W.; Liebthal, M.F.; Gerken, M.; Schnitzer, H.; Mueller, S.M.; Dietz, K.-J. The Chloroplast 2-Cysteine Peroxiredoxin Functions as Thioredoxin Oxidase in Redox Regulation of Chloroplast Metabolism. *Elife* **2018**, *7*, doi:10.7554/eLife.38194.
20. Buchanan, B.B. The Ferredoxin/Thioredoxin System: A Key Element in the Regulatory Function of Light in Photosynthesis. *Bioscience* **1984**, *34*, 378–383.
21. Gontero, B.; Avilan, L.; Lebreton, S. Control of carbon fixation in chloroplasts. In *Control of Primary Metabolism in Plants*; Plaxton, W.C., McManus, M.T., Eds.; Blackwell Publishing Ltd: Oxford, UK, 2006; pp. 187–218 ISBN 978-0-470-98864-0.

22. Gontero, B.; Maberly, S.C. An Intrinsically Disordered Protein, CP12: Jack of All Trades and Master of the Calvin Cycle. *Biochem. Soc. Trans.* **2012**, *40*, 995–999, doi:10.1042/BST20120097.
23. Graciet, E.; Gans, P.; Wedel, N.; Lebreton, S.; Camadro, J.-M.; Gontero, B. The Small Protein CP12: A Protein Linker for Supramolecular Complex Assembly. *Biochemistry* **2003**, *42*, 8163–8170, doi:10.1021/bi034474x.
24. Avilan, L.; Puppo, C.; Erales, J.; Woudstra, M.; Lebrun, R.; Gontero, B. CP12 Residues Involved in the Formation and Regulation of the Glyceraldehyde-3-Phosphate Dehydrogenase-CP12-Phosphoribulokinase Complex in *Chlamydomonas Reinhardtii*. *Mol Biosyst* **2012**, *8*, 2994–3002, doi:10.1039/c2mb25244a.
25. Mcfarlane, C.; Shah, N.; Kabasakal, B.V.; Cotton, C.A.R.; Bubeck, D.; Murray, J.W. Structural Basis of Light-Induced Redox Regulation in the Calvin Cycle. *PNAS* **2019**, *116*, 20984–20990, doi:10.1101/414334.
26. Yu, A.; Xie, Y.; Pan, X.; Zhang, H.; Cao, P.; Su, X.; Chang, W.; Li, M. Photosynthetic Phosphoribulokinase Structures: Enzymatic Mechanisms and the Redox Regulation of the Calvin-Benson-Bassham Cycle. *Plant Cell* **2020**, *32*, 1556–1573, doi:10.1105/tpc.19.00642.
27. Groben, R.; Kaloudas, D.; Raines, C.A.; Offmann, B.; Maberly, S.C.; Gontero, B. Comparative Sequence Analysis of CP12, a Small Protein Involved in the Formation of a Calvin Cycle Complex in Photosynthetic Organisms. *Photosynth. Res.* **2010**, *103*, 183–194, doi:10.1007/s11120-010-9542-z.
28. Stanley, D.N.; Raines, C.A.; Kerfeld, C.A. Comparative Analysis of 126 Cyanobacterial Genomes Reveals Evidence of Functional Diversity among Homologs of the Redox-Regulated CP12 Protein. *Plant Physiol.* **2013**, *161*, 824–835, doi:10.1104/pp.112.210542.
29. Fermani, S.; Trivelli, X.; Sparla, F.; Thumiger, A.; Calvaresi, M.; Marri, L.; Falini, G.; Zerbetto, F.; Trost, P. Conformational Selection and Folding-upon-Binding of Intrinsically Disordered Protein CP12 Regulate Photosynthetic Enzymes Assembly. *J. Biol. Chem.* **2012**, *287*, 21372–21383, doi:10.1074/jbc.M112.350355.
30. Launay, H.; Barré, P.; Puppo, C.; Manneville, S.; Gontero, B.; Receveur-Bréchot, V. Absence of Residual Structure in the Intrinsically Disordered Regulatory Protein CP12 in Its Reduced State. *BBRC* **2016**, *477*, 20–26, doi:10.1016/j.bbrc.2016.06.014.
31. Launay, H.; Barré, P.; Puppo, C.; Zhang, Y.; Maneville, S.; Gontero, B.; Receveur-Bréchot, V. Cryptic Disorder out of Disorder: Encounter between Conditionally Disordered CP12 and Glyceraldehyde-3-Phosphate Dehydrogenase. *J. Mol. Biol.* **2018**, *430*, 1218–1234, doi:10.1016/j.jmb.2018.02.020.
32. Shao, H.; Huang, W.; Avilan, L.; Receveur-Brechot, V.; Puppo, C.; Puppo, R.; Lebrun, R.; Gontero, B.; Launay, H. A New Type of Flexible CP12 Protein in the Marine Diatom *Thalassiosira Pseudonana*. *CCS* **2021**, *18*, doi:10.21203/rs.3.rs-135099/v1.
33. Adamski, W.; Salvi, N.; Maurin, D.; Magnat, J.; Milles, S.; Jensen, M.R.; Abyzov, A.; Moreau, C.; Blackledge, M. A Unified Description of Intrinsically Disordered Protein Dynamics under Physiological Conditions Using NMR Spectroscopy. *J. Am. Chem. Soc.* **2019**, doi:10.1021/jacs.9b09002.
34. Pauwels, K.; Lebrun, P.; Tompa, P. To Be Disordered or Not to Be Disordered: Is That Still a Question for Proteins in the Cell? *Cell. Mol. Life Sci.* **2017**, 1–20, doi:10.1007/s00018-017-2561-6.
35. Bodart, J.-F.; Wieruszeski, J.-M.; Amniai, L.; Leroy, A.; Landrieu, I.; Rousseau-Lescuyer, A.; Vilain, J.-P.; Lippens, G. NMR Observation of Tau in *Xenopus Oocytes*. *J. Magn. Reson.* **2008**, *192*, 252–257, doi:10.1016/j.jmr.2008.03.006.
36. Theillet, F.-X.; Binolfi, A.; Bekei, B.; Martorana, A.; Rose, H.M.; Stuiver, M.; Verzini, S.; Lorenz, D.; van Rossum, M.; Goldfarb, D.; et al. Structural Disorder of Monomeric α-Synuclein Persists in Mammalian Cells. *Nature* **2016**, *530*, 45–50, doi:10.1038/nature16531.

37. Banci, L.; Barbieri, L.; Luchinat, E.; Secci, E. Visualization of Redox-Controlled Protein Fold in Living Cells. *Chemistry & Biology* **2013**, *20*, 747–752, doi:10.1016/j.chembiol.2013.05.007.
38. Mercatelli, E.; Barbieri, L.; Luchinat, E.; Banci, L. Direct Structural Evidence of Protein Redox Regulation Obtained by In-Cell NMR. *Biochim. Biophys. Acta* **2016**, *1863*, 198–204, doi:10.1016/j.bbamcr.2015.11.009.
39. Hwang, T.L.; van Zijl, P.C.; Mori, S. Accurate Quantitation of Water-Amide Proton Exchange Rates Using the Phase-Modulated CLEAN Chemical EXchange (CLEANEX-PM) Approach with a Fast-HSQC (FHSQC) Detection Scheme. *J. Biomol. NMR* **1998**, *11*, 221–226.
40. Delaglio, F.; Grzesiek, S.; Vuister, G.W.; Zhu, G.; Pfeifer, J.; Bax, A. NMRPipe: A Multidimensional Spectral Processing System Based on UNIX Pipes. *J. Biomol. NMR* **1995**, *6*, 277–93, doi:10.1007/BF00197809.
41. Lee, W.; Tonelli, M.; Markley, J.L. NMRFAM-SPARKY: Enhanced Software for Biomolecular NMR Spectroscopy. *Bioinformatics* **2015**, *31*, 1325–1327, doi:10.1093/bioinformatics/btu830.
42. Eaton, J.; Bateman, D.; Haubert, S.; Wehbring, R. GNU Octave Version 4.2.1 Manual: A High-Level Interactive Language for Numerical Computations; 2017;
43. Xu, S.; Ni, S.; Kennedy, M.A. NMR Analysis of Amide Hydrogen Exchange Rates in a Pentapeptide-Repeat Protein from *A. Thaliana*. *Biophysical Journal* **2017**, *112*, 2075–2088, doi:10.1016/j.bpj.2017.04.016.
44. Zhang, Y.-Z. Protein and Peptide Structure and Interactions Studied by Hydrogen Exchanger and NMR, PhD thesis, University of Pennylvania, 1995.
45. Piotukh, K.; Kosslick, D.; Zimmermann, J.; Krause, E.; Freund, C. Reversible Disulfide Bond Formation of Intracellular Proteins Probed by NMR Spectroscopy. *Free Radic. Biol. Med.* **2007**, *43*, 1263–1270, doi:10.1016/j.freeradbiomed.2007.06.010.
46. Mochizuki, A.; Saso, A.; Zhao, Q.; Kubo, S.; Nishida, N.; Shimada, I. Balanced Regulation of Redox Status of Intracellular Thioredoxin Revealed by In-Cell NMR. *JACS* **2018**, *140*, 3784–3790, doi:10.1021/jacs.8b00426.
47. Kruger, N.J. The Bradford Method for Protein Quantitation. *Methods Mol Biol* **1994**, *32*, 9–15, doi:10.1385/0-89603-268-X:9.
48. Ferrage, F.; Zoonens, M.; Warschawski, D.E.; Popot, J.; Bodenhausen, G. Slow Diffusion of Macromolecular Assemblies by a New Pulsed Field Gradient NMR Method. *Journal of the American Chemical Society* **2003**, *125*, 2541–2545.
49. Ferraro, D.M.; Lazo, N.D.; Robertson, A.D. EX1 Hydrogen Exchange and Protein Folding. *Biochemistry* **2004**, *43*, 587–594, doi:10.1021/bi035943y.
50. Cierpicki, T.; Otlewski, J. Amide Proton Temperature Coefficients as Hydrogen Bond Indicators in Proteins. *J. Biomol. NMR* **2001**, *21*, 249–261.
51. Trainor, K.; Palumbo, J.A.; MacKenzie, D.W.S.; Meiering, E.M. Temperature Dependence of NMR Chemical Shifts: Tracking and Statistical Analysis. *Protein Science* **2020**, *29*, 306–314, doi:https://doi.org/10.1002/pro.3785.
52. Dujardin, M.; Madan, V.; Gandhi, N.S.; Cantrelle, F.-X.; Launay, H.; Huvent, I.; Bartenschlager, R.; Lippens, G.; Hanoulle, X. Cyclophilin A Allows the Allosteric Regulation of a Structural Motif in the Disordered Domain 2 of NS5A and Thereby Fine-Tunes HCV RNA Replication. *J. Biol. Chem.* **2019**, *294*, 13171–13185, doi:10.1074/jbc.RA119.009537.
53. Selvaratnam, R.; Chowdhury, S.; VanSchouwen, B.; Melacini, G. Mapping Allostery through the Covariance Analysis of NMR Chemical Shifts. *PNAS* **2011**, *108*, 6133–6138, doi:10.1073/pnas.1017311108.
54. Cavanagh, J.; Fairbrother, W.; Palmer, A.G.; Rance, M.; Skelton, N. *Principles and Practice: Protein NMR Spectroscopy*; Second edition.; ISBN 978-0-12-164491-8.

55. Marri, L.; Trost, P.; Pupillo, P.; Sparla, F. Reconstitution and Properties of the Recombinant Glyceraldehyde-3-Phosphate Dehydrogenase/CP12/Phosphoribulokinase Supramolecular Complex of Arabidopsis. *Plant Physiol* **2005**, *139*, 1433–1443, doi:10.1104/pp.105.068445.
56. Clement, R.; Lignon, S.; Mansuelle, P.; Jensen, E.; Pophillat, M.; Lebrun, R.; Denis, Y.; Puppo, C.; Maberly, S.C.; Gontero, B. Responses of the Marine Diatom *Thalassiosira Pseudonana* to Changes in CO2 Concentration: A Proteomic Approach. *Sci Rep* **2017**, *7*, 42333, doi:10.1038/srep42333.
57. Elena López-Calcagno, P.; Omar Abuzaid, A.; Lawson, T.; Anne Raines, C. Arabidopsis CP12 Mutants Have Reduced Levels of Phosphoribulokinase and Impaired Function of the Calvin–Benson Cycle. *J Exp Bot* **2017**, *68*, 2285–2298, doi:10.1093/jxb/erx084.
58. Howard, T.P.; Fryer, M.J.; Singh, P.; Metodiev, M.; Lytovchenko, A.; Obata, T.; Fernie, A.R.; Kruger, N.J.; Quick, W.P.; Lloyd, J.C.; et al. Antisense Suppression of the Small Chloroplast Protein CP12 in Tobacco Alters Carbon Partitioning and Severely Restricts Growth. *Plant Physiol.* **2011**, *157*, 620–631, doi:10.1104/pp.111.183806.
59. Li, K.; Qiu, H.; Zhou, M.; Lin, Y.; Guo, Z.; Lu, S. Chloroplast Protein 12 Expression Alters Growth and Chilling Tolerance in Tropical Forage *Stylosanthes Guianensis (Aublet) Sw*. *Front Plant Sci* **2018**, *9*, 1319, doi:10.3389/fpls.2018.01319.
60. Dietz, K.-J. Redox Signal Integration: From Stimulus to Networks and Genes. *Physiologia Plantarum* **2008**, *133*, 459–468, doi:https://doi.org/10.1111/j.1399-3054.2008.01120.x.
61. Buchanan, B.B.; Balmer, Y. REDOX REGULATION: A Broadening Horizon. *Annual Review of Plant Biology* **2005**, *56*, 187–220, doi:10.1146/annurev.arplant.56.032604.144246.
62. Jensen, M.R.; Ruigrok, R.W.; Blackledge, M. Describing Intrinsically Disordered Proteins at Atomic Resolution by NMR. *Current Opinion in Structural Biology* **2013**, *23*, 426–435, doi:10.1016/j.sbi.2013.02.007.
63. Gurrieri, L.; Del Giudice, A.; Demitri, N.; Falini, G.; Pavel, N.V.; Zaffagnini, M.; Polentarutti, M.; Crozet, P.; Marchand, C.H.; Henri, J.; et al. Arabidopsis and Chlamydomonas Phosphoribulokinase Crystal Structures Complete the Redox Structural Proteome of the Calvin-Benson Cycle. *Proc. Natl. Acad. Sci. U.S.A.* **2019**, *116*, 8048–8053, doi:10.1073/pnas.1820639116.
64. Marri, L.; Zaffagnini, M.; Collin, V.; Issakidis-Bourguet, E.; Lemaire, S.D.; Pupillo, P.; Sparla, F.; Miginiac-Maslow, M.; Trost, P. Prompt and Easy Activation by Specific Thioredoxins of Calvin Cycle Enzymes of *Arabidopsis Thaliana* Associated in the GAPDH/CP12/PRK Supramolecular Complex. *Mol. Plant* **2009**, *2*, 259–269, doi:10.1093/mp/ssn061.
65. Marri, L.; Pesaresi, A.; Valerio, C.; Lamba, D.; Pupillo, P.; Trost, P.; Sparla, F. In Vitro Characterization of Arabidopsis CP12 Isoforms Reveals Common Biochemical and Molecular Properties. *Journal of Plant Physiology* **2010**, *167*, 939–950, doi:10.1016/j.jplph.2010.02.008.
66. Yoshida, K.; Hara, A.; Sugiura, K.; Fukaya, Y.; Hisabori, T. Thioredoxin-Like2/2-Cys Peroxiredoxin Redox Cascade Supports Oxidative Thiol Modulation in Chloroplasts. *PNAS* **2018**, *115*, E8296, doi:10.1073/pnas.1808284115.
67. Faustino, A.F.; Barbosa, G.M.; Silva, M.; Castanho, M.A.R.B.; Da Poian, A.T.; Cabrita, E.J.; Santos, N.C.; Almeida, F.C.L.; Martins, I.C. Fast NMR Method to Probe Solvent Accessibility and Disordered Regions in Proteins. *Scientific Reports* **2019**, *9*, 1647, doi:10.1038/s41598-018-37599-z.
68. Launay, H.; Receveur-Bréchot, V.; Carrière, F.; Gontero, B. Orchestration of Algal Metabolism by Protein Disorder. *Arch. Biochem. Biophys.* **2019**, *672*, 108070, doi:10.1016/j.abb.2019.108070.
69. Bhowmick, A.; Brookes, D.H.; Yost, S.R.; Dyson, H.J.; Forman-Kay, J.D.; Gunter, D.; Head-Gordon, M.; Hura, G.L.; Pande, V.S.; Wemmer, D.E.; et al. Finding Our Way in the Dark Proteome. *J. Am. Chem. Soc.* **2016**, *138*, 9730, doi:10.1021/jacs.6b06543.

70. Teilum, K.; Olsen, J.G.; Kragelund, B.B. Globular and Disordered – the Non-Identical Twins in Protein-Protein Interactions. *Front. Mol. Biosci.* **2015**, *2*, doi:10.3389/fmolb.2015.00040.
71. Baalmann, E.; Scheibe, R.; Cerff, R.; Martin, W. Functional Studies of Chloroplast Glyceraldehyde-3-Phosphate Dehydrogenase Subunits A and B Expressed in *Escherichia Coli*: Formation of Highly Active A4 and B4 Homotetramers and Evidence That Aggregation of the B4 Complex Is Mediated by the B Subunit Carboxy Terminus. *Plant Mol Biol* **1996**, *32*, 505–513, doi:10.1007/BF00019102.
72. Thieulin-Pardo, G.; Avilan, L.; Kojadinovic, M.; Gontero, B. Fairy "Tails": Flexibility and Function of Intrinsically Disordered Extensions in the Photosynthetic World. *Front. Mol. Biosci.* **2015**, *2*, 23, doi:10.3389/fmolb.2015.00023.
73. Zhang, Y.; Launay, H.; Liu, F.; Lebrun, R.; Gontero, B. Interaction between Adenylate Kinase 3 and Glyceraldehyde-3-Phosphate Dehydrogenase from *Chlamydomonas Reinhardtii*. *FEBS J.* **2018**, *285*, 2495–2503, doi:10.1111/febs.14494.
74. Lemaire, S.D.; Quesada, A.; Merchan, F.; Corral, J.M.; Igeno, M.I.; Keryer, E.; Issakidis-Bourguet, E.; Hirasawa, M.; Knaff, D.B.; Miginiac-Maslow, M. NADP-Malate Dehydrogenase from Unicellular Green Alga *Chlamydomonas Reinhardtii*. A First Step toward Redox Regulation? *Plant Physiol* **2005**, *137*, 514–521, doi:10.1104/pp.104.052670.
75. Mackinder, L.C.M.; Chen, C.; Leib, R.D.; Patena, W.; Blum, S.R.; Rodman, M.; Ramundo, S.; Adams, C.M.; Jonikas, M.C. A Spatial Interactome Reveals the Protein Organization of the Algal CO2-Concentrating Mechanism. *Cell* **2017**, *171*, 133-147.e14, doi:10.1016/j.cell.2017.08.044.
76. Wunder, T.; Cheng, S.L.H.; Lai, S.-K.; Li, H.-Y.; Mueller-Cajar, O. The Phase Separation Underlying the Pyrenoid-Based Microalgal Rubisco Supercharger. *Nat Commun* **2018**, *9*, doi:10.1038/s41467-018-07624-w.
77. Freeman Rosenzweig, E.S.; Xu, B.; Kuhn Cuellar, L.; Martinez-Sanchez, A.; Schaffer, M.; Strauss, M.; Cartwright, H.N.; Ronceray, P.; Plitzko, J.M.; Förster, F.; et al. The Eukaryotic CO2-Concentrating Organelle Is Liquid-like and Exhibits Dynamic Reorganization. *Cell* **2017**, *171*, 148-162.e19, doi:10.1016/j.cell.2017.08.008.
78. Choi, Y.H.; van Spronsen, J.; Dai, Y.; Verberne, M.; Hollmann, F.; Arends, I.W.C.E.; Witkamp, G.-J.; Verpoorte, R. Are Natural Deep Eutectic Solvents the Missing Link in Understanding Cellular Metabolism and Physiology? *Plant Physiol.* **2011**, *156*, 1701–1705, doi:10.1104/pp.111.178426.
79. Dai, Y.; Varypataki, E.M.; Golovina, E.A.; Jiskoot, W.; Witkamp, G.-J.; Choi, Y.H.; Verpoorte, R. Chapter Seven - Natural deep eutectic solvents in plants and plant cells: In vitro evidence for their possible functions. In *Advances in Botanical Research*; Verpoorte, R., Witkamp, G.-J., Choi, Y.H., Eds.; Eutectic Solvents and Stress in Plants; Academic Press, 2021; Vol. 97, pp. 159–184.
80. Brillouet, J.-M.; Verdeil, J.-L.; Odoux, E.; Lartaud, M.; Grisoni, M.; Conéjéro, G. Phenol Homeostasis Is Ensured in Vanilla Fruit by Storage under Solid Form in a New Chloroplast-Derived Organelle, the Phenyloplast. *Journal of Experimental Botany* **2014**, *65*, 2427–2435, doi:10.1093/jxb/eru126.
81. Marri, L.; Sparla, F.; Pupillo, P.; Trost, P. Co-Ordinated Gene Expression of Photosynthetic Glyceraldehyde-3-Phosphate Dehydrogenase, Phosphoribulokinase, and CP12 in *Arabidopsis Thaliana*. *J Exp Bot* **2005**, *56*, 73–80, doi:10.1093/jxb/eri020.
82. Rochaix, J.D. *Chlamydomonas Reinhardtii* as the Photosynthetic Yeast. *Annu Rev Genet* **1995**, *29*, 209–230, doi:10.1146/annurev.ge.29.120195.001233.
83. Kastritis, P.L.; O'Reilly, F.J.; Bock, T.; Li, Y.; Rogon, M.Z.; Buczak, K.; Romanov, N.; Betts, M.J.; Bui, K.H.; Hagen, W.J.; et al. Capturing Protein Communities by Structural Proteomics in a Thermophilic Eukaryote. *Mol. Syst. Biol.* **2017**, *13*, 936, doi:10.15252/msb.20167412.

84. Ellis, R.J. Macromolecular Crowding: An Important but Neglected Aspect of the Intracellular Environment. *Curr Opin Struct Biol* **2001**, *11*, 114–119, doi:10.1016/s0959-440x(00)00172-x.
85. Ellis, R.J. Macromolecular Crowding: Obvious but Underappreciated. *Trends in Biochemical Sciences* **2001**, *26*, 597–604, doi:10.1016/S0968-0004(01)01938-7.
86. Zimmerman, S.B.; Trach, S.O. Estimation of Macromolecule Concentrations and Excluded Volume Effects for the Cytoplasm of Escherichia Coli. *J Mol Biol* **1991**, *222*, 599–620, doi:10.1016/0022-2836(91)90499-v.
87. Christiansen, A.; Wang, Q.; Cheung, M.S.; Wittung-Stafshede, P. Effects of Macromolecular Crowding Agents on Protein Folding in Vitro and in Silico. *Biophys Rev* **2013**, *5*, 137–145, doi:10.1007/s12551-013-0108-0.
88. Li, C.; Charlton, L.; Lakkavaram, A.; Seagle, C.; Wang, G.; Young, G.; MacDonald, J.; Pielak, G. Differential Dynamical Effects of Macromolecular Crowding on an Intrinsically Disordered Protein and a Globular Protein: Implications for in-Cell NMR Spectroscopy. *J Am Chem Soc* **2008**, *130*, 6310–6311, doi:10.1021/ja801020z.
89. Wang, Y.; Benton, L.A.; Singh, V.; Pielak, G.J. Disordered Protein Diffusion under Crowded Conditions. *J Phys Chem Lett* **2012**, *3*, 2703–2706, doi:10.1021/jz3010915.
90. Luchinat, E.; Banci, L. In-Cell NMR: A Topical Review. *IUCrJ* **2017**, *4*, 108–118, doi:10.1107/S2052252516020625.
91. Cedeño, C.; Pauwels, K.; Tompa, P. Protein Delivery into Plant Cells: Toward In Vivo Structural Biology. *Front Plant Sci* **2017**, *8*, doi:10.3389/fpls.2017.00519.
92. Küken, A.; Sommer, F.; Yaneva-Roder, L.; Mackinder, L.C.; Höhne, M.; Geimer, S.; Jonikas, M.C.; Schroda, M.; Stitt, M.; Nikoloski, Z.; et al. Effects of Microcompartmentation on Flux Distribution and Metabolic Pools in *Chlamydomonas Reinhardtii* Chloroplasts. *Elife* **2018**, *7*, doi:10.7554/eLife.37960.